Snow cover modeling on glaciers

An attempt at a high-resolution model chain for mass balance calculation

Master's Thesis

in Atmospheric Sciences

Submitted to the
Faculty of Geo- and Atmospheric Sciences
of the
University of Innsbruck

in partial fulfillment of the requirements for the degree of
Master of Science

by
Peter Ehrengruber

Advisors

Dr. Sascha Bellaire,
Dr. Lindsey Nicholson

Innsbruck, December 2017

Abstract

With the growing importance of the earth's climate and how it is evolving over recent decades, glaciers, since they are good indicators of predominant climate conditions, are of growing interest for scientific research. One of the most meaningful variables describing a glaciers development is its mass balance. However, its calculation usually involves a good amount of field work and gathering measurement data. To simplify the process, a new approach combining weather forecast data with snowpack modelling was developed. This allows for mass balance calculations in very remote areas without the need for lengthy and expensive field work.

The goal of this study was, to assess whether combining a high-resolution snowpack model with a high-resolution numerical weather prediction model would make a viable and accurate approach for glacier mass balance modelling. As a high-resolution snowpack model, SNOWPACK was used, while the meteorological forecast data was provided by COSMO-1. The study was conducted on Hochjochferner, a glacier on the border of Austria and Italy. For verification, data of an Automated Weather Station (AWS) situated on the surface of Hochjochferner was available, as well as snow stake measurements from 6 different locations on Hochjochferner. Before SNOWPACK was run with COSMO-data, it was tested using the AWS data and compared to the snow height measurements by the AWS and ablation measurements at the snow stakes. All modelling was done over the course of the hydrological year 2014/15, spanning from 01/10/2014 to 30/09/2015. As a reference, a manual glacier mass balance done with a combination of stake data and terrestrial photography was used.

At first, SNOWPACK was run at the location of the AWS, to find out the optimal model setup and compare it to the in-situ snow height and ablation measurements. At the end of the ablation season, SNOWPACK had modelled 0.16 m more ablation compared to the stake measurements, which translates to an error of 3.6 %.

As a second step, all meteorological parameters necessary to run SNOWPACK were extrapolated from the AWS location to all stake locations. This was done with the help of MeteoIO, a library capable of processing meteorological input and output data. SNOWPACK was then run at these locations, to determine whether the extrapolations produce realistic input data that can be used to force SNOWPACK, and to compare the results to the snow stake measurements. Afterwards, the AWS data was extrapolated to 19 virtual mass balance points distributed over the whole glacier surface, dividing it into elevation bands with an equidistance of 50 m. Again, SNOWPACK was run at these points, and a glacier mass balance was calculated off of the results. The obtained mean specific mass balance overestimated ablation by 450 mm w.e., an error of 20.6 %.

As the final step, COSMO-data was introduced to force the model. Meteorological

data was extracted from the model for the 6 grid points closest to the glacier, and interpolated to the location and elevation of the desired points. Again, it was first tested at the AWS location, before running the model at the 6 snow stake locations and, finally, at the 19 virtual mass balance points to obtain a glacier-wide annual mass balance. The resulting mean specific mass balance overestimated ablation by 1040 mm w.e., an error of 51 %.

After comprehensive error analysis, it can be said that the reason for this error can most likely be found in the COSMO-data itself, namely a positive bias in relative humidity, coupled with a negative bias in temperature. The model chain was run once more using the same settings, only with substituting humidity data provided by COSMO with the humidity data measured by the AWS. This resulted in a much lower mean specific mass balance error of 11.9 %.

Thus, although the resulting error being significant at first, it seems that much more accurate results can be gained with minor adjustment of certain parameters, to compensate for an underlying systematic error. Which means that, after more testing and analysis preferably at different research sites, this approach could indeed make a viable and accurate alternative for glacier mass balance calculation, and considerably ease the process as well as lower the amount of work typically required.

Contents

1 Introduction

1.1 Motivation

The earth's cryosphere in general, and glaciers in particular, are a more and more discussed and relevant topic in today's society and media. On a regional scale, one reason for this is that in mountainous regions like the Alps, glaciers influence the lives of the people living there. Glacial run-off is often the main water supply for glaciated valleys. In dry regions of the Himalayas (Immerzeel et al. 2013) or the Andes (Vuille et al. 2008), it can be the only source of drinking water for some very large and populated zones (Jiménez Cisneros et al. 2014).

But the main reason for the growing popularity, is that glaciers turned out to be very good indicators of the earth's climate and how it is changing over the last decades. Especially mountain glaciers, with their comparatively small scale, are very sensitive to changes in the prevailing climate and respond quickly to variations in temperature and precipitation (Oerlemans and Fortuin 1992). This fact makes the topic one of global importance, simply because the ongoing climate change already is one of the most politically discussed topics around the world and will affect everybody in one way or another. The earth's climate system is very complex and dynamic, and small changes in one part can quickly amplify and lead to very big effects in another.

For example: An important part of climate change are the - globally speaking - rising temperatures. Warmer temperatures lead to melting in parts of the cryosphere all over the world, be it mountain glaciers, permafrost soil or the big ice sheets on Greenland and Antarctica. Mountain glaciers worldwide are showing a trend of retreat and homogeneous mass loss (Zemp et al. 2015). This releases water into the oceans, and results in a rise of the global mean sea level, which in turn causes coastal zones to be threatened by flooding. The displacement of climate zones and precipitation patterns in the future could have drastic effects on population zones and agriculture around the world. These processes are already ongoing, and will continue to become more and more important as the climate keeps changing (Vaughan et al. 2013; Wong et al. 2014).

The points described above are exactly why knowledge about the cryosphere has become more and more important in science as well. Monitoring glacier behaviour all over the world helps us understand climate change and its effects on a global scale, and provides some useful insight into the evolvement of the past, present and, partly, the future climate.

One of the most important parameters describing the condition and development of a glacier is its mass balance. According to Moelg et al. (2008), it is the most direct

link between the underlying atmospheric forcing and the volume response of a glacier. It can be positive or negative, and indicates how much ice mass a given glacier has gained or lost over a specific time period - usually a year.

For scientific purpose, the best possible scenario would be to measure the exact mass balance of every glacier in the world, every year. But the process of measuring the mass balance of even a single glacier is either very laborious or very expensive, depending on the chosen method. Additionally, many of the earth's glaciers are situated in very remote areas and quite difficult to get to. Therefore, systematic and long-term mass balance measurements are only performed on a small number of glaciers with relatively easy access. This made another approach to assess a glacier's mass balance a necessity: by modelling.

There are already several developed methods to model glacier mass balance (see section 1.2). One thing they have in common, is that ideally on-site measurement data of the most influential meteorological parameters (mainly temperature and precipitation) is available as an input to the model. The only option not requiring local field work is to use area-wide available meteorological data, e.g. from satellite measurements or numerical weather prediction (NWP) models. But because they're operating on a global scale, the resolution of these models is traditionally too low for small-scale glaciological use. Furthermore, they usually have some difficulties providing accurate precipitation values over complex terrain like mountain ranges. However, in recent years we are seeing more high-resolution NWP as well as snowpack models being available. The increased resolution improved the weather forecasting, especially in complex terrain (Schirmer and Jamieson 2015), which could make combining two of those models to calculate glacier mass balance (GMB) a viable, flexible, accurate and inexpensive alternative approach. How well this works, and to which degree of accuracy, will be the main subject of this thesis.

1.2 State of Research

The recording of glacier length measurements in the European Alps started very early, with the longest record being the one of Unterer Grindelwaldgletscher, starting back in 1534. But despite - or even because of - the early start, data from this era is sparse and far in between, and it was not until the 19th century that glaciologists started to systematically record annual glacier lengths of several glaciers across the Alps (Oerlemans 2005; Leclercq and Oerlemans 2012).

GMB measurement, however, did not start before 1874, when it was done for the first time on Rhône Glacier in Switzerland (Mercanton 1916). It took more than another half a century for a systematic approach to the study of glacier mass balance to be developed, which happened in the 1940s (Dyurgerov and Meier 1997). Nowadays,

one of the main sources for global collected GMB measurements is the *Glacier Mass Balance Bulletin* (GMBB), edited by the World Glacier Monitoring Service (WGMS) in Zurich. The latest volume, GMBB 12, states that for the years 2009/10 and/or 2010/11, basic mass balance information of 126 glaciers was reported (Zemp et al. 2013).

Over the years, several methods and approaches for modelling the GMB have been developed. They vary greatly in complexity and range, from simple temperature index models to physically based surface energy balance calculations that try to resolve all the physical processes at work. Hoelzle et al. (2003) for example tried to derive GMB just from cumulative glacier length changes. Marzeion et al. (2012) also used a very simple model based on monthly values of temperature and precipitation, while Huss et al. (2008) worked with an increased resolution of daily values. Another tried and tested approach is the degree-day model, which is based on the relation between ablation and air temperature. It calculates the sum of positive air temperatures over a certain time interval, and derives the amount of melting via a proportional *degree-day factor* (Hock 2003; Kuhn 2008). While these models at first glance seem to oversimplify the processes at work, they usually yield surprisingly accurate results (Ohmura 2001).

Probably the most comprehensive method of modelling GMB is via a physical-based model quantifying the surface energy balance (SEB) of the glacier in question. All energy fluxes that occur at the glacial surface are calculated using available meteorological data, most of the time from an automated weather station (AWS) situated directly on or in the vicinity of the glacier in question. The sum of those fluxes make up the SEB, which states if the total energy flux is either to or from the glacier surface. From this, the amount of melt that is taking place can be derived.

One of the first GMB-models using this approach was done by Oerlemans and Hoogendoorn (1989). A little later, a two-dimensional model investigating the mass and surface energy balance on Morteratschgletscher was developed by Klok and Oerlemans (2002).

The first numerical, high-resolution snowpack model (CROCUS) was developed by Brun et al. (1989). In 2002, Bartelt and Lehning (2002) presented their SNOWPACK model, which is also the one used in this thesis. Those models were originally developed with avalanche forecasting in mind and are therefore tailored to the specific needs of seasonal snowpacks. The first application of SNOWPACK to a glacierized area to calculate the SEB and GMB was done by Michlmayr et al. (2008).

The idea of coupling such models with input data from a NWP model is still rather new, and there is not a lot of studies utilizing this approach. Bellaire et al. (2011) tried to use a similar model chain for the Canadian avalanche warning system, and continued with this approach to forecast weak layers in the seasonal snowpack (Bellaire and Jamieson 2013; Horton and Jamieson 2016). To the authors knowledge,

to date there is no study using such a model chain for glaciological use and mass balance calculation.

1.3 Objective and outline

The main objective of this thesis is to find out to what degree of accuracy glacier mass balance can be modelled using data from a numerical weather prediction model as an input to a high-resolution snowpack model. For this purpose, the SEB will first be resolved at a single point using available AWS data and SNOWPACK. As a next step, the SEB will then be calculated at strategically placed locations at the glacier surface of Hochjochferner, using extrapolation methods as a way to adjust the meteorological parameters to the respective location and elevation. Finally, instead of measured AWS data, COSMO-1 data will be used as an input. COSMO-1 is a NWP model with a horizontal resolution of 1 km. Using this data, the mass balance for the whole glacier will be calculated. The results will be compared to the measured mass balance of Hochjochferner, and the biggest sources of errors will be addressed.

Research questions:

- To which degree of accuracy can the measured ablation of Hochjochferner be recreated with SNOWPACK and the use of AWS data at a single point?
- To which degree of accuracy can the measured mass balance of Hochjochferner be recreated using SNOWPACK and suitable extrapolation methods for the AWS data?
- How big is the difference between the measured mass balance of Hochjochferner and the modelled MB using COSMO data as an input and SNOWPACK to resolve the surface energy balance?

2 Physical Background

2.1 Glacier Mass Balance

A typical mountain glacier stretches over a few hundred meters of vertical elevation, which means that it is exposed to considerable variations in meteorological parameters. This is why a healthy glacier can be compartmentalized into two zones (Fig. 2.1). In the *Accumulation area*, the glacier gains mass. There is a permanent snow-cover on the surface of the glacier, which prevents melting of the underlying ice. After a densification process, the snow will convert into firn and further into ice. Accumulation encompasses everything that leads to mass gain, the main sources being solid precipitation and avalanches. Other processes that lead to accumulation include snow redistribution through wind, deposition and refreezing of water. The *Ablation area* is characterized by the seasonal melting of the snow cover. Without the protection of the snow, the ice is directly exposed to the overlying atmosphere and the sun, which leads to melting and mass loss in this area. In most cases, by far the most important process leading to ablation is melting. Other processes include sublimation, calving and, again, snow redistribution. Separating those two areas is the *Equilibrium Line Altitude (ELA)*. Despite the name, this is not a fixed altitude for every glacier, but rather a line that delimits the accumulation from the ablation zone. Because of inhomogeneities in terrain and local shading, the ELA can be higher in some parts of a glacier than in others.

The imbalance between the mass gain in the accumulation zone and the mass loss

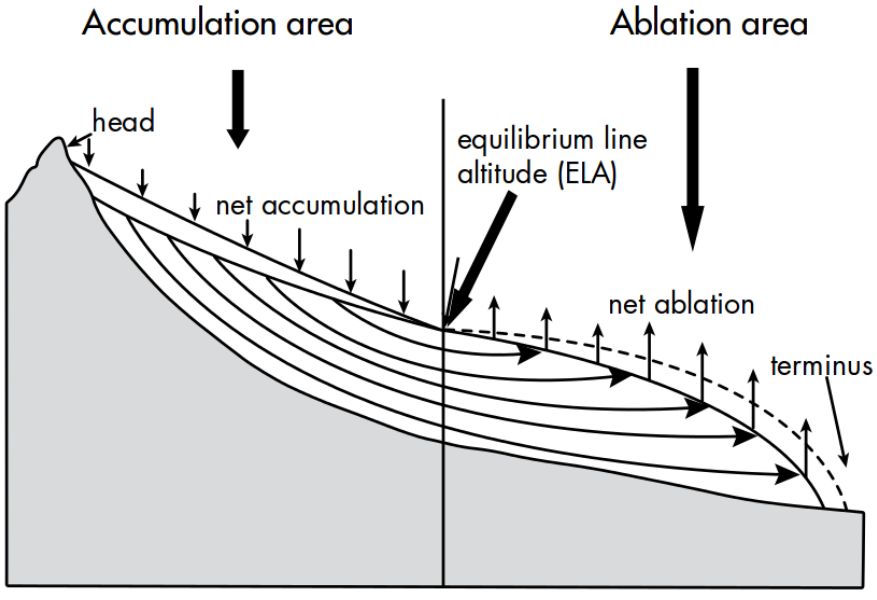

Figure 2.1: Sketch of a mountain glacier, cross section along the flow line. (Armstrong 2010)

in the ablation zone is balanced by the flow of the glacier, which transfers mass from the accumulation to the ablation area. If total mass gain equals total mass loss over an annual cycle, the glacier is in a state of equilibrium. The sum of those mass exchanges is called the *Mass Balance*. Although mass exchange not only happens at the glacier surface, but also internally (ice - water transitions) and at the interface between ice and ground (basal melting), the surface mass exchange is usually bigger then the latter two by several orders of magnitude, which is why they can be safely neglected for the purpose of this thesis.

The thickness change over time $\dot{h}$ of a column of ice at any point on a glacier can be expressed as the sum of:

- The local mass balance $\dot{b}/\rho$, and
- the local, horizontal gradient of ice flux ∇q

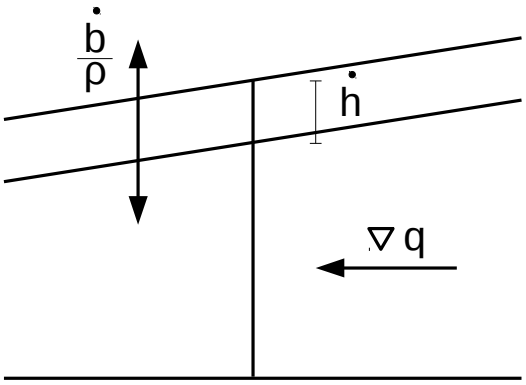

Figure 2.2: The thickness change over time $\dot{h}$ of a column of ice at any point on a glacier. (Kaser et al. 2003)

Therefore, using the continuity equation of ice, $\dot{h}$ can be expressed as

$$\dot{h} = \frac{\dot{b}}{\rho} - \nabla q, \qquad [\mathrm{m}] \quad (2.1)$$

where $\dot{b}$ is the local mass balance rate and ρ is the ice density. Using Eq. 2.1, the specific mass balance rate at a single fixed point on a glacier can be written as:

$$\dot{b} = \rho(\dot{h} + \nabla q). \qquad [\mathrm{kg\ m^{-2}}] \quad (2.2)$$

Regarding the mass balance, three different types can be distinguished:

- Specific Mass Balance $\dot{b}$ [kg/m^2 or $mm\ w.e.$]

- Total Mass Balance B $[kg/m^2]$
- Mean Specific Mass Balance $\bar{b}$ $[kg/m^2$ or $mm\ w.e.]$

A mass balance always incorporates a time component as well, which was deliberately neglected in the units given above. This is because it is up to the user to decide over which time frame the mass balance is calculated. Usually, and also in this study, the mass balance is measured (or modelled) over the time span of a hydrological year, which, in the European Alps, is defined from 1st October until 30th September of the following year. It is then called the *Annual Mass Balance*.

The total mass balance is defined as the specific mass balance of every point on the glacier surface integrated over its horizontal area A:

$$B = \int_A \dot{b}\ dA. \qquad [\text{kg m}^{-2}] \quad (2.3)$$

If the total mass balance of a glacier is continuously negative, it will shrink, retreat and disappear in the long run. Likewise, if it keeps having a positive mass balance, it will grow and expand. The time frame in which this happens varies with the size and location of the glacier, and can span anything from decades to millennia.

The mean specific mass balance removes the dependency on the glacier size, and is a relative value which makes it easy to compare mass balance values between different glaciers:

$$\bar{b} = B/A. \qquad [\text{kg m}^{-2}] \quad (2.4)$$

All of the above are usually - for comparability and convenience - converted into millimetres of water equivalent (mm w.e.) via a density assumption. The resulting value is the height of the water column that would be created if the ice was melted.

There are several widely used methods of determining the mass balance of a glacier, mainly depending on which data one has available. For this study, the glaciological method will be used. It will be described in detail in chapter 3.3.2.

2.2 Surface Energy Balance

Since the mass balance modelling in this study is done with SNOWPACK, which calculates ablation by resolving the Surface Energy Balance, a short introduction to the concept of a surface energy balance on a glacier and its components will be given here.

Generally speaking, an energy balance can be calculated at an interface where energy is exchanged, in this case the atmosphere-ground-interface. The *Surface Energy Balance (SEB)* discussed here is nothing else than the sum of all energy fluxes that

pass through the interface (in this case the glacier surface), either from the atmosphere to the snow/ice-body or vice versa. If the glacial body gains energy, it heats up, which leads to melting. The interface is assumed to be infinitesimally thin and without mass or heat capacity. Thus, energy is directly transferred between the two surrounding bodies. As discussed in the previous section about mass balance, the glacial body naturally also experiences internal and basal energy fluxes. But, as for mass balance, the magnitude of these processes in the setting of this study is comparatively small and can therefore once more safely be neglected.

The SEB of an open, flat snow or ice surface is given by (in units of $[Wm^{-2}]$):

$$dE/dt = S_I + S_O + L_I + L_O + H_S + H_L + P + G, \tag{2.5}$$

where dE/dt is the change rate of the snow or ice body's internal energy, S_I is the incoming and S_O the reflected shortwave radiation, L_I and L_O are the incoming and outgoing longwave radiation respectively, H_S is the sensible heat flux, H_L is the latent heat flux, P is the heat flux created by precipitation and G is the ground heat flux - the ground being a body of snow and/or ice in this case. The prefix of each one of these terms differs in literature depending on the perspective. For this thesis, we look at the energy budget of the snow or ice body, so fluxes that lead to energy gain in said body are defined as positive, while energy fluxes that deduct energy are defined as negative. Likewise, dE/dt is positive if the glacier receives energy, and vice versa. Below, each of the fluxes will be described shortly.

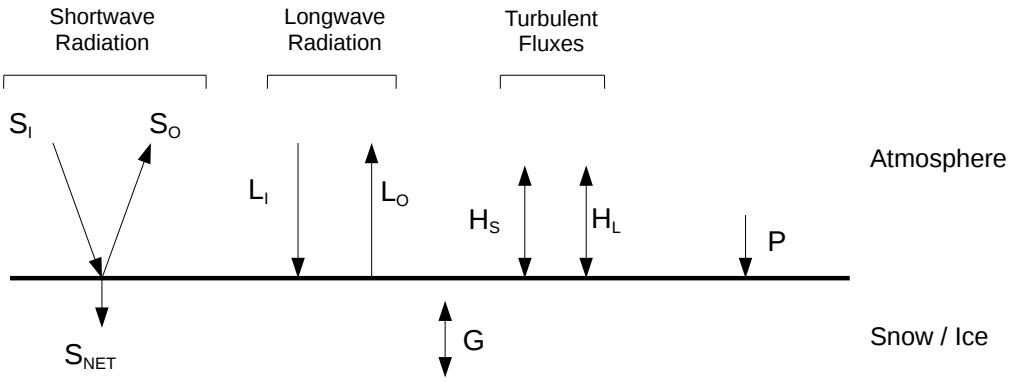

Figure 2.3: Components of the Surface Energy Balance

Looking at Figure 2.3, starting from the left, S_I and S_O are the shortwave radiation fluxes. They are created by solar radiation, and usually are the biggest terms in Equation (2.5). S_I is the incoming solar radiation, and the biggest energy source for

a glacier. It can be divided in a direct and a diffuse (outgoing shortwave radiation reflected back by the environment) part and varies greatly depending on solar zenith angle (which in turn depends on the time of the day and the season), cloud cover, elevation and slope aspect. S_O is the reflected part of solar radiation. It depends on S_I and on the albedo α of the surface with the relation

$$S_O = S_I \alpha. \qquad [\mathrm{Wm}^{-2}] \quad (2.6)$$

The albedo is a dimensionless number indicating the reflectiveness of a surface, and on a glacier can vary greatly from around 0.95 (for new snow) down to 0.2 (for dirty glacier ice). S_{NET} is the resulting net shortwave radiation that goes into the ice body and is defined by

$$S_{NET} = S_I - S_O. \qquad [\mathrm{W\ m}^{-2}] \quad (2.7)$$

Next are the longwave radiation fluxes L_I and L_O. The emitted longwave radiation of any surface can be calculated with the use of the Stefan-Boltzmann equation:

$$L = \epsilon \sigma T^4, \qquad [\mathrm{W\ m}^{-2}] \quad (2.8)$$

where ϵ is the emissivity of the radiating body, which in the case of snow/ice can be assumed as $\epsilon = 1$, and $\sigma = 5.67 \cdot 10^{-8}$ [W m^{-2}K^{-4}] is the Stefan-Boltzmann constant. L_I is the incoming longwave radiation, which is emitted by the atmosphere and depends primarily on the air temperature T_a in its lower few hundred meters. Additionally, any longwave radiation that is emitted by the ground (L_O) but reflected by the atmosphere due to cloudiness is also included in this term. L_O is the outgoing longwave radiation, which is determined by the temperature of the emitting surface T_S. On a glacier, the surface temperature can by definition not exceed 0°C.

The four radiative energy fluxes described above can be brought together to calculate the *Net Radiative Flux*:

$$R_{NET} = S_I + S_O + L_I + L_O, \qquad [\mathrm{W\ m}^{-2}] \quad (2.9)$$

which, with the help of Equation 2.6, can be written as:

$$R_{NET} = S_I \cdot (1 - \alpha) + (L_I + L_O). \qquad [\mathrm{W\ m}^{-2}] \quad (2.10)$$

R_{NET} in itself is a good indicator of the SEB, as the remaining fluxes usually are comparatively small. Because L_I and L_O are often of the same magnitude, R_{NET} is highly dependant on the albedo α. With a low α and a reasonably high S_I, R_{NET} is always going to be positive, and the snowpack will gain energy.

H_S and H_L are the turbulent heat fluxes. They are driven by turbulent eddies in the surface boundary layer, which can transport either heat (H_S) or moisture (H_L) to and from the glacier surface. The sensible heat flux H_S is given by:

$$H_S = \rho_a c_{p,a} \overline{w' T'_a}, \qquad [\mathrm{W\ m}^{-2}] \quad (2.11)$$

where ρ_a is the air density, $c_{p,a}$ is the specific heat of air at a constant pressure, w is the vertical component of the wind velocity in the surface boundary layer and T_a the air temperature. The sensible heat flux is highly dependant on the temperature gradient between the surface and the air temperature in the lower boundary layer, and is thus greatest on warm summer days. The latent heat flux H_L accounts for heat that is transferred in the form of moisture (either by sublimation or deposition) and can be written as:

$$H_L = \rho_a L_{vi} \overline{w'Q'}, \qquad [\mathrm{W\ m^{-2}}] \quad (2.12)$$

where L_{vi} is the latent heat for sublimation of ice at 0°C and Q is the specific humidity. The latent heat flux, analogue to H_S, is very dependant on the vapour pressure gradient at the surface and is therefore greatest in the case of dry air over a water saturated surface.

P is the heat flux due to precipitation falling on the glacier surface. It can transport energy either in sensible or latent form, but is usually very small. One exception would be a case of warm rain falling onto and penetrating a cold snowpack, which only happens on very rare occasions.

Finally, G is the ground heat flux. It can be towards the surface or away from it (albeit with a different sign to all the other fluxes as it is coming from the other side of the interface), and it depends on how the temperature gradient inside the ice body is changing over time. If the snowpack or the glacier are temperate, $G = 0$.

2.3 SNOWPACK

SNOWPACK was originally developed by the Swiss Federal Institute for Snow and Avalanche Research (SLF) in Davos, Switzerland, to support the swiss avalanche warning system and forecast (Lehning et al. 1999). It is a numerical, one-dimensional physical snowpack model, which means it neglects lateral transfers and only resolves vertical gradients and transfers. Snow is modelled as a three-phase porous material with the components ice, air, and water. As it was developed with avalanche research applications in mind, where the layering of a snowpack is of utmost importance, it resolves the snowpack in great detail by dividing it into layers. Those layers are defined by the snow microstructure, and between them, all the occurring transfers and fluxes are modelled.

Each of the snow layers is defined by a few state variables: density, temperature and the volumetric fractions of the three phases of water, which are dimensionless and

$$\theta_i + \theta_w + \theta_a = 1, \quad (2.13)$$

where θ is the volumetric fraction of ice (i), water (w) and moist air (a), respectively.

Additionally, each layer is defined by four primary snow microstructure parameters (which can be derived from the state variables): grain size, bond size, dendricity and sphericity of the contained snow crystals (Lehning et al. 2002b). While grain size and bond size (which is the size of the bonds in between single snow crystals) are given in [mm], dendricity and sphericity are dimensionless parameters between 0 and 1, which state how spheric or dendric the snow crystal is. For example, new snow normally has a dendricity of 1 and a sphericity of 0, while an old and completely round snow crystal has a sphericity of 1 and a dendricity of 0. These parameters are used to accurately model the microstructure of the snow and its metamorphic developments, and they evolve over time by modelling equilibrium growth metamorphism and kinetic metamorphism for each timestep. With the help of the microstructural parameters above, the macroscopic properties of each layer can be calculated: thermal conductivity and viscosity. Those properties are important for further microstructural processes taking place in the snowpack which do not need to be described here. With these snow properties defined and calculated, the core equations that govern the model can be resolved: mass conservation, energy conservation and snowpack settling.

The model uses a Lagrangian coordinate system, which is not stationary but follows the ice matrix as settling occurs. This brings several advantages over a classic Eulerian coordinate system, and eases the computation of the conservation equations considerably. The most important advantage is the knowledge of the history of the medium, as the layers don't exchange mass - if a layer gets thinner, the coordinate system simply moves with it. This is critical in avalanche research applications, as very thin weak layers can develop in the model and be easily identified (Lehning et al. 2002a). Since the model is based on the finite-element method, and displacement field continuity is required in a Lagrangian formulation, new layers (i.e. new snow) can just be added on top of the grid.

The last important part are the boundary conditions at the bottom and the top of the snowpack. The ground boundary condition allows for discharge of melt water, which is important in a classical snowpack-on-soil-environment as well as for glacier mass balance modelling. Meltwater is generally stored in a layer until the layer reaches its maximum water content (which depends on the physical properties of the layer). When the maximum is reached, any excess water is then moved to the adjacent lower layer. Once the water reaches the bottom layer, it is discharged and leaves the system. The top boundary condition can be twofold:

- A Dirichlet boundary condition, which takes the surface temperature as a value measured by an automated weather station or any other method of reliable surface temperature measurement

- A Neumann boundary condition, which resolves the surface energy balance (as

discussed in Chapter 2.2).

For ablation periods ($T_S = 0°$ C), the Neumann boundary condition is used. If the Dirichlet condition would be used in this case, the true energy input would be underestimated, as the surface temperature is always zero during ablation periods. Thus, when T_S approaches melting temperature, the model switches and uses the Neumann boundary condition - which is the case for the important periods in this study when ablation takes place (Bartelt and Lehning 2002). Without the availability of a measured surface temperature however, the Dirichlet boundary condition cannot be applied, which is why at all locations other than the AWS site, the model has to be run with the Neumann boundary condition anyway. Therefore, to ensure consistence and comparability between the results, simulations at the AWS site were also done in the same way.

2.4 COSMO

COSMO, which stands for Consortium for Small Scale Modelling, is a nonhydrostatic, limited-area atmospheric prediction model. Being a nonhydrostatic model, it solves the full vertical momentum equation and is therefore able to also accurately model processes generated through vertical flow (e.g. thunderstorms). Its basic version has been developed by the German Meteorological Service (*Deutscher Wetterdienst*, DWD). Nowadays, it aims to be a high-resolution model for regional weather forecast, and is regularly run at resolutions as low as 1 km.

The COSMO-data used for this study was provided by the Federal Office of Meteorology and Climatology MeteoSwiss, where the model is currently run at two different horizontal resolutions: 7 km (COSMO-7) and 1 km (COSMO-1).

As the aim of this study was to force SNOWPACK with a high-resolution numerical weather prediction model, COSMO-1 was used. It is operational since the beginning of 2014, albeit being run pre-operationally before March 2016, which means there were still occasional changes being made. It features a horizontal grid point spacing of 1.1 km (0.01°) as well as 80 layers from the ground to the top of the atmosphere. At present, it is the highest-resolution model which is run regularly for the greater Alps area. It is run 8 times a day for t + 33 hours, and once a day for t + 45 hours. It is nested in (which means the initial conditions are taken from) ECMWF's global IFS-HRES model, which has a horizontal resolution of 10 km. Available meteorological variables are provided every 10 minutes.

The main advantage of a high-resolution model is the better representation of real topography in the model surface, leading to better inclusion of local phenomena like thunderstorms or thermal wind systems in the forecast. But also one of the most important meteorological parameters for GMB-modelling, precipitation, should be depicted

more accurately. Therefore, it should provide the best possible input data quality for this study. NWP models in general have difficulties with accurately predicting precipitation, especially over complex, mountainous terrain like the study area (Schirmer and Jamieson 2015; Buzzi 2008). COSMO-1 delivers better results than its predecessor COSMO-2, however, still has sometimes considerable errors (Morsier 2015).

3 Data and Methods

3.1 Study site

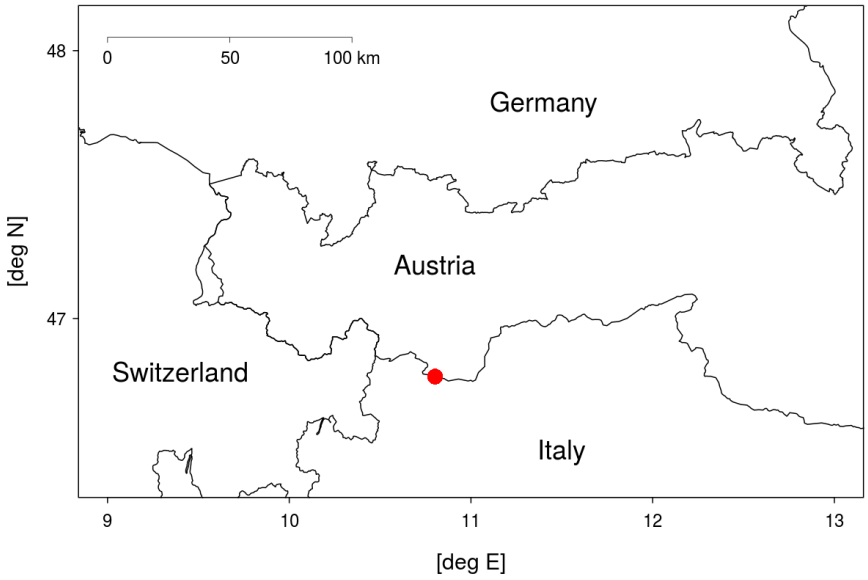

Figure 3.1: The red point marks the location of the Study site

The study focuses on Hochjochferner, a glacier located at the border of Italy and Austria, in a mountain group called the Ötztal Alps in Tyrol (see Fig. 3.1). The Hochjochferner flows down on the Austrian side of the border to the north and north-west, into the Rofen-Valley, and stretches from the summit of Grawandspitze (3251 m a.s.l.), which denotes the south-westernmost point of the glacier, past Fineilspitze (3514 m a.s.l.) and further to the east. Its aspect is mostly NW, and the length along the flow line from the Grawandspitze down to the terminus of the main tongue is 2.8 km. At the point of its greatest thickness, the ice measures around 45 m (Fischer et al. 2014). It spans an area of 6 km^2, and from its highest to its lowest point has an elevation difference of 900 meters. Instead of having one large accumulation area and one big tongue, Hochjochferner has a rather complex topography and is divided into 5 independent accumulation areas. But because of the terrain, 2 out of the 3 glacier tongues finish at around 2900 m. The main tongue with its very prominent middle moraine flows down to 2700 m a.s.l. (see Fig. 3.3).

The Automated Weather Station (AWS) providing the in-situ data for this study is operated by the Utrecht University's Institute for Marine and Atmospheric Research (IMAU), and was put on site in September 2011. It has since been taken down in September 2016 and is not recording any more data. It was situated on the westernmost

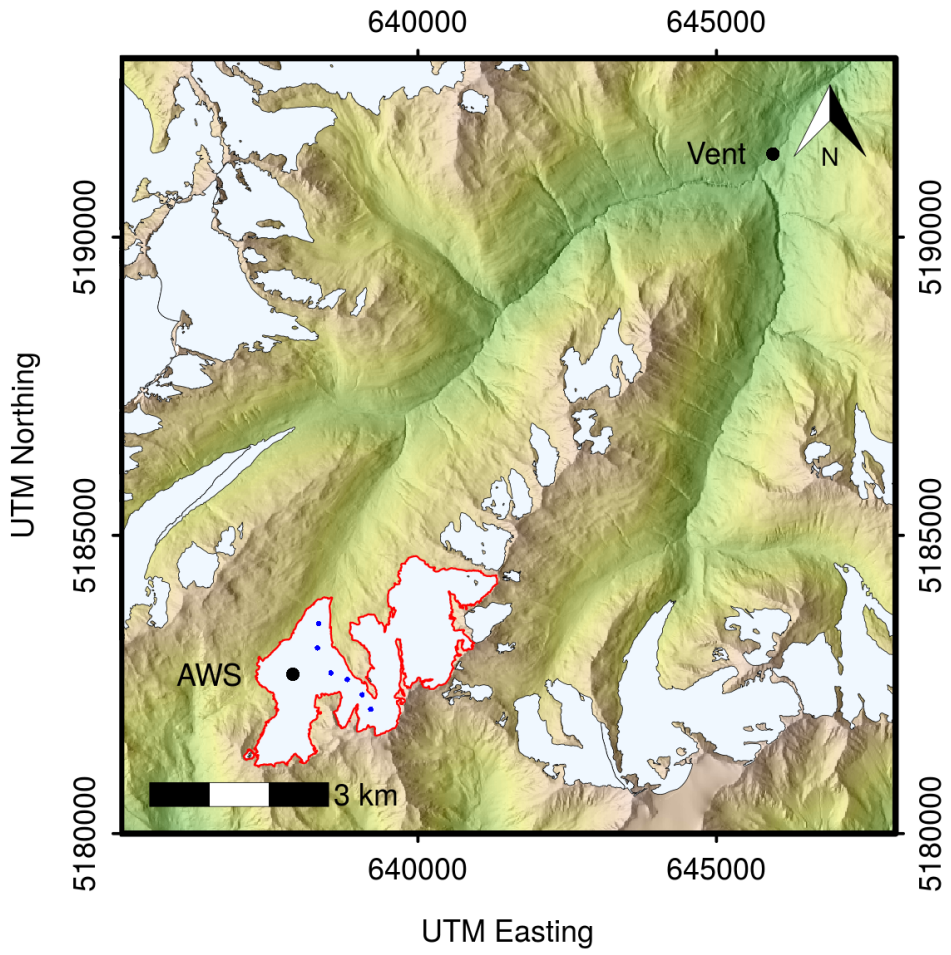

Figure 3.2: The Hochjochferner area. In the top right corner is Vent. The red area marks the Hochjochferner as specified by the Austrian Glacier Inventory 2006, the black marker the position of the Automated Weather Station (AWS). The small blue dots represent the snow stakes.

(orographically speaking left) part of the glacier tongue, at an elevation of 2860 m a.s.l. Its exact position is marked by the black dot in Figure 3.2). It recorded data of air temperature, air pressure, wind speed and direction, incoming and outgoing short- and longwave radiation, moisture data and snow height via a sonic altimeter. It also featured tilt and roll angle measurements to determine whether the station was tilted because of strong or uneven ice melt during ablation season. The station was not drilled into the ice but positioned on a tripod, which means the sonic altimeter could not deliver meaningful measurements for ice ablation. However, during the study period, several snow stakes were drilled and measured multiple times a year (one of them in direct vicinity to the AWS), so the ablation-data is still reliable. Most of these snow stakes, which were used for verification of the extrapolated, simulated mass balances, are located along the flow line of the western part of Hochjochferner.

The study site features a relatively dry, inner-alpine climate regime. 11 km air-line

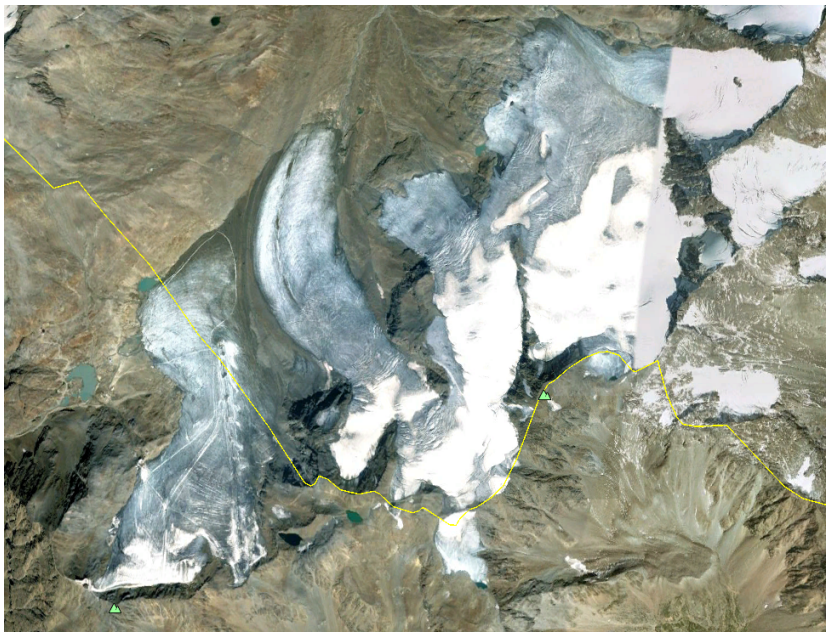

Figure 3.3: Satellite Image composition of Hochjochferner. The image date of the left 3/4ths of the image is 12th August 2003, the right 1/4th was taken on 1st January 2000 n(the border is visible at the glacier area). The yellow line marks the Austrian-Italian border (Source: Google Earth).

distance from Hochjochferner, located in the Rofen-Valley, is Vent, where an AWS run by the University of Innsbruck is located (see Fig. 3.2). It records a mean annual precipitation of 680 mm.

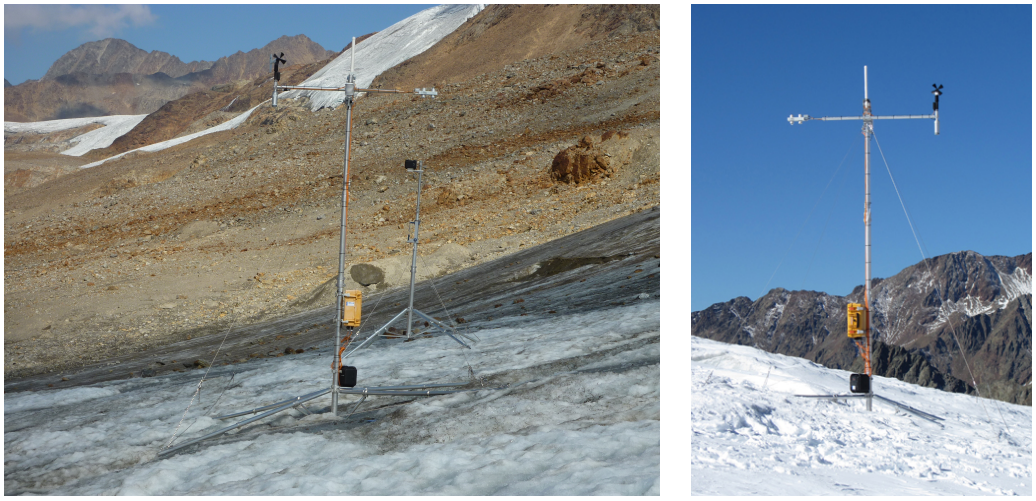

Figure 3.4: The AWS on Hochjochferner (Source: G. Kaser (left) and Utrecht University (right)).

3.2 Data

In this chapter, an overview over each of the datasets will be given, as well as some basic analysis. Several datasets were used over the course of this study:

- AWS data of Hochjochferner, which was kindly provided by the Utrecht University's Institute for Marine and Atmospheric Research (IMAU),
- snow stake data of Hochjochferner, provided by the Ice and Climate group of University of Innsbrucks Institute of Atmospheric and Cryospheric Sciences,
- COSMO-1 forecast data, provided by the Federal Office of Meteorology and Climatology MeteoSwiss,
- a digital elevation model (DEM) of the study site.

Since the full range of data (AWS data, stake measurements and COSMO-1 data) was only available for one hydrological year (October 2014 - September 2015), the study will focus solely on this time span, as it would not make much sense to introduce additional error sources to an environment that already has and unknown degree of uncertainties using a NWP model for a very localized application.

3.2.1 AWS data

AWS data provided by Utrecht University was available from the 12th September 2011 to the 26th November 2015. With the definition of a hydrological year from 1st October to 30th September, the data spans 4 complete accumulation-ablation-cycles.

Parameter	Sensor type	Accuracy	Sampling [min]
Temperature	Vaisala HMP45C	0.4 °C at -20 °C	5
Humidity	Vaisala HMP45C	2 % (RH < 90 %)	5
Radiation Shield	Young 41003	-	-
Wind Speed	05103-L R.M. Young	0.3 ms^{-1}	5
Wind Direction	05103-L R.M. Young	3 deg	5
Net Radiation	Kipp Zonen CNR1	Daily Total ±10 %	5
Surface Height	SR50 Height Ranger	0.01 m	30-60
Pressure	Vaisala PTB101B	4 hPa	30-60
Data Logger	Campbell CR10	-	-
Batteries	Tadiran 3.6 V, 35 Ah	-	-
Data Logger Temp	Campbell	0.1 deg	30-60
Battery Voltage	Campbell	0.1 V	30-60

Table 3.1: Sensors and their accuracy and sampling intervals used at the AWS.

Unfortunately, there were issues with the AWS between July 2013 and July 2014 and the data was lost, and was filled with ARGOS satellite data for this timespan. The sensors used and their specifications can be seen in Tab. 3.1.

The dataset covers hourly values of air temperature, relative and specific humidity, wind speed and direction, all 4 components of the radiation budget (incoming and outgoing long- and shortwave radiation), air pressure and snow height measurements, amongst others. These hourly values are half-hour averages of five- to thirty-minutes-interval-measurements (depending on the sensor) for 15 minutes before and after every full hour. The dataset was mostly complete, with a few data gaps (maximum data gap size was n = 11 hours), which were interpolated with suitable methods described below. Basic quality control to remove obvious faulty measurement spikes was already done by the Institute for Marine and Atmospheric Research.

3.2.1.1 Air Temperature

As the AWS is located at 2860 m a.s.l., temperatures are relatively low year-round. The average temperature for the study period is -1.5 °C, and for 6 out of 12 months, monthly average is below zero (see Fig. 3.5). The absolute maximum is 15.8 °C (reached in July 2015), the absolute minimum -22.4 °C (December 2014). Because of its location on a glacier, the prevailing winds and the terrain, the mean diurnal variations in air temperature are relatively low (on average 5.3 degrees between daily minimum and maximum). As can be seen in Figure 3.5, 2014/15 in general, and especially the ablation season, was noticeably warmer than the years before. In July 2015 for example, the monthly mean (8.8 °C) was 4.5 °C higher than the one of July during the "record summer" 2013 (4.3 °C). Because of the sinusoidal nature of daily temperature curves, missing values were interpolated with cubic spline interpolation.

3.2.1.2 Surface Temperature

Surface Temperature was calculated by using the measured outgoing longwave radiation:

$$T_S = \sqrt[4]{\frac{L_O}{\epsilon\sigma}}, \qquad [\mathrm{K}] \quad (3.1)$$

where ϵ is the emissivity of snow or ice (taken as $\epsilon = 1$) and $\sigma = 5.67 \cdot 10^{-8}$ $[Wm^{-2}K^{-4}]$ is the Stefan-Boltzmann constant.

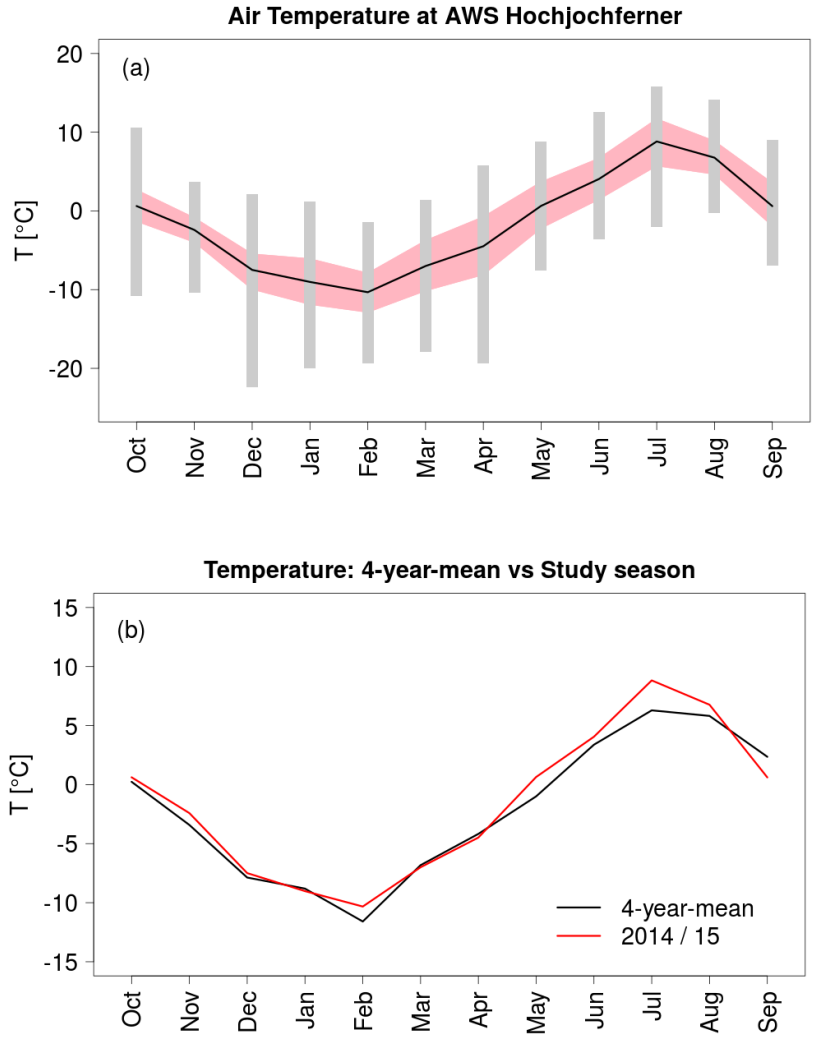

Figure 3.5: **(a):** Monthly mean air temperatures for the study period at the AWS location (black line). Absolute monthly maxima and minima are denoted by the grey bars, while mean monthly maxima and minima are shown by the red background. **(b):** Comparison of air temperature 4-year mean values (2011 - 2015, black) and 2014/15 values (red).

3.2.1.3 Precipitation and Humidity

Since there is no rain gauge included with the AWS, measured precipitation values are obtained via snow height. This of course includes only solid precipitation, which partly explains the very low values for July and August (Fig. 3.6). A fixed conversion value of 90 kgm^{-3} was used to transform centimetres snow height to millimetres water equivalent. This new snow density value was measured on the site of the AWS station on 1st October 2015. The night before it snowed 20 cm with an air temperature of around -4 °C.

Generally speaking, there is precipitation during all seasons. Compared to the years before, 2014/15 had slightly more solid precipitation, mainly due to a very wet

November 2014. Relative humidity (RH) values were truncated at 100 % and, because of their coupling to air temperature, missing values were also interpolated with cubic spline interpolation. Specific humidity values, which were only really used for the computation of the latent heat flux in the SEB, were interpolated between the values at the same daytime 2 days before and after. This was done because the continually changing airmasses yielded gross overestimations of specific humidity values when using a cubic spline interpolation rhythm.

Snow height measurements with a sonic altimeter are prone to errors, which range from a moving station and different reflection properties depending on the surface, to poor data quality during precipitation events. Especially during heavy snowfall, the

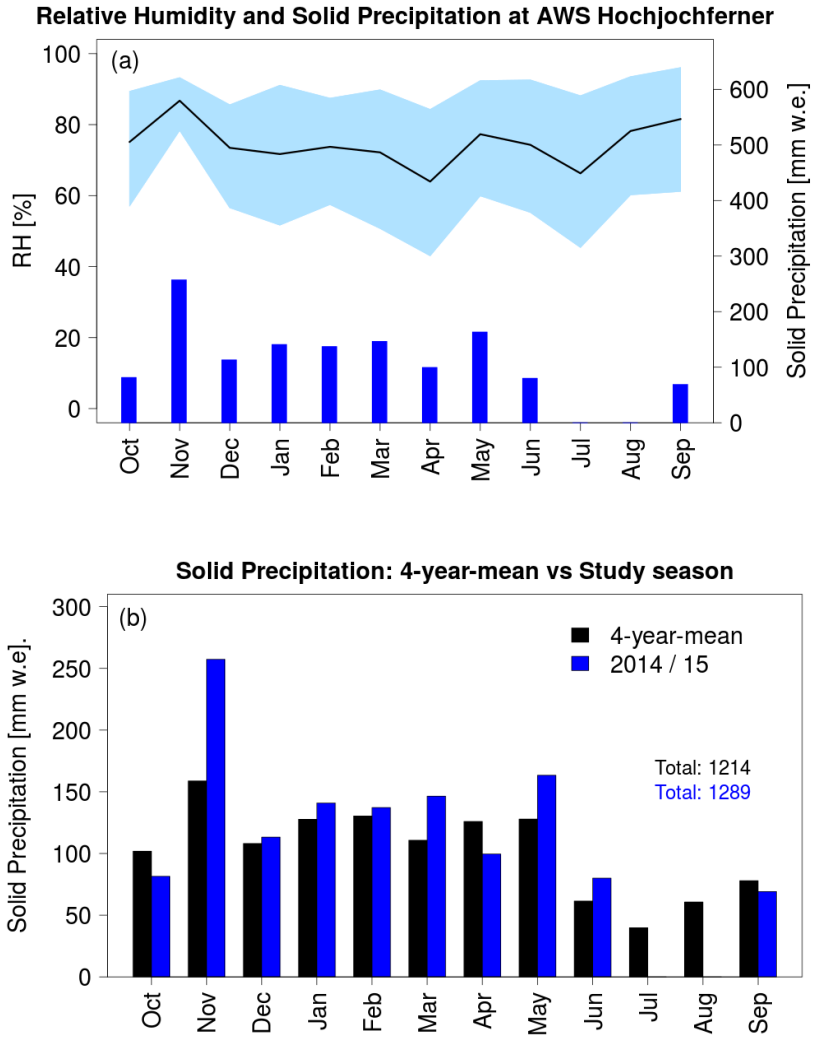

Figure 3.6: **(a):** Monthly mean relative humidity (black line) with monthly mean maxima and minima (blue background), together with monthly sums of the water equivalent of solid precipitation (blue bars). **(b):** Comparison of solid precipitation 4-year mean values (2011 - 2015, black bars) and 2014/15 values (blue).

signal often gets reflected not by the ground, but instead by falling or blowing snow that is in the air between the sensor and the surface, causing false height values to be recorded. Additionally, it is very important for SNOWPACK to only get "real" solid precipitation data. Otherwise, even minimal "false" height gains stemming from processes like nocturnal meltwater refreezing would lead to an interpretation of fresh snowfall, which in turn would lead to false albedo values and reduced melting rates. Therefore, a rather lengthy approach to prepare snow height measurement data was taken. At first, missing data points were linearly interpolated. Afterwards, to remove spikes and measurement irregularities mainly during ablation season, values lying outside the 95%-quantile were set to the respective 95%-limits, which introduced a set height value to be the "zero"-level during ablation season, getting rid of the height measurement noise. To remove incorrect measurements especially during snowfall events, a 5cm-height-gain-threshold was introduced, removing values that were >5cm higher than the hourly value before and afterwards (both conditions had to be true) and instead interpolating linearly between the 2 adjacent values. This took out a lot of the mentioned misreadings due to falling or blowing snow by assuming a snowfall rate >5 cm/h has to be a false measurement. To include snow height gain only from snowfall events, a RH-threshold was introduced, removing snow height gains when RH < 90%. Finally, because snowfall was still significantly overestimated during precipitation events (the reason being lots of small spikes because of irregular measurements), values were smoothed during precipitation events so SNOWPACK could work with the data. This was done by introducing a 3-hour running mean:

$$H_x = \frac{H_{x-1} + H_{x+1}}{2}, \qquad [\mathrm{m}] \quad (3.2)$$

where H_x is the respective hourly snow height measurement at timestep x.

Since the total accumulated snow height for each precipitation event and season was known, the results were compared to those values to ensure the model was run with the correct amounts of snowfall. In Fig. 3.7, two snow height graphs for the first two weeks of November 2014 can be seen; one before (black) and one after(red) the described smoothing and filtering process.

3.2.1.4 Radiation Data

Detailed plots for radiation data will be given in Chapter 4.1. Here, only data treatment will be discussed. Incoming shortwave radiation (ISWR) values were set to zero if the corresponding outgoing shortwave radiation (OSWR) value was zero, and between 20:00 and 03:00 UTC (21:00 and 04:00 CET). Missing values were interpolated with a mean of the values at the same hour two days before and after. OSWR was set to zero if ISWR was zero as well. For missing values, daily mean albedo α_d was

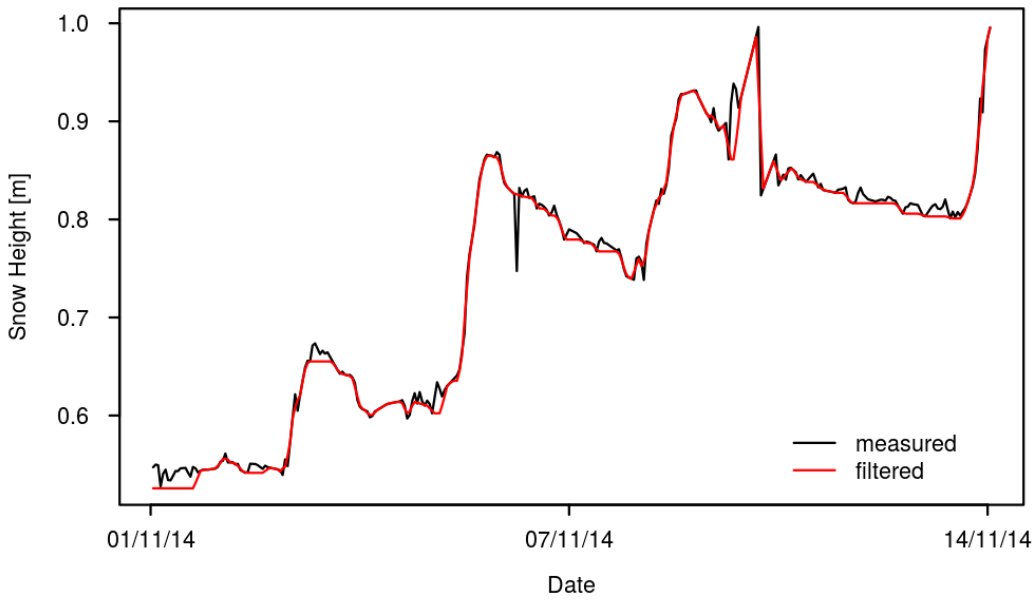

Figure 3.7: Comparison of snow height data before (black) and after the smoothing process for the first two weeks of November 2014.

calculated for each day, and missing OSWR values were set to

$$OSWR = ISWR \cdot \alpha_d. \qquad [\mathrm{W\ m^{-2}}] \quad (3.3)$$

Finally, to avoid misreadings because of a snow-covered ISWR-sensor, for the cases where $ISWR < OSWR$ and solar zenith angle was low (10:00 - 15:00 CET), ISWR was set to

$$ISWR = \frac{OSWR}{\alpha_d}. \qquad [\mathrm{W\ m^{-2}}] \quad (3.4)$$

Missing longwave radiation values were interpolated with cubic spline interpolation.

3.2.1.5 Wind

With the station situated on a glacier, one would expect that it is heavily influenced by katabatic wind systems. This is however not the case, since the glacier slope is oriented north - south, and the maxima in the wind direction distribution are located in the westerly and easterly sector, as can be seen in Figure 3.8. The reason is the surrounding terrain; the glacier is located in a flat and not very pronounced saddle. The topography is dropping down towards the Schnals Valley to the west, which is why altitude wind influence is dominating at the station. Because of this, a "same-as-last-day"-approach for filling missing values did not seem justifiable. Additionally, data gaps were small, which is why the missing values were linearly interpolated for wind speed as well as wind direction data. The mean wind speed for the study period is 3.7

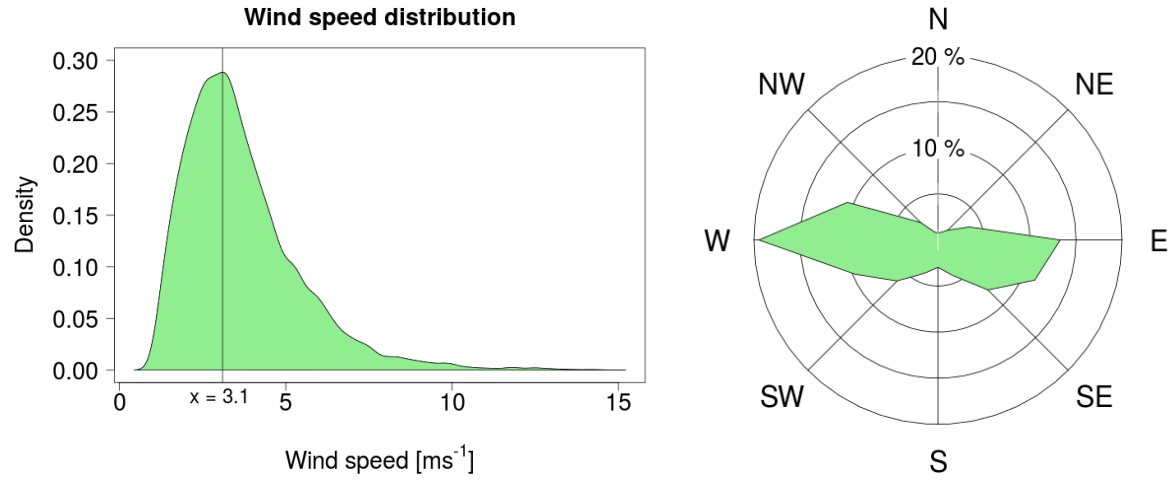

Figure 3.8: Wind speed (left) and direction (right) distribution at the AWS location. The vertical line in the left graph is located at the maximum of the frequency distribution (3.1 m s^{-1}).

m s^{-1}, with the maximum of the frequency distribution at 3.1 m s^{-1}. The seasonal absolute maximum is at 15.4 m s^{-1}.

3.2.2 Snow Stake Data

The snow stakes on Hochjochferner were in place during the summers of 2014 and 2015, spanning two seasons of ablation data. Eight stakes were put up on the main tongue of the glacier, and one stake was put around 20 m to the west of the AWS (Stake

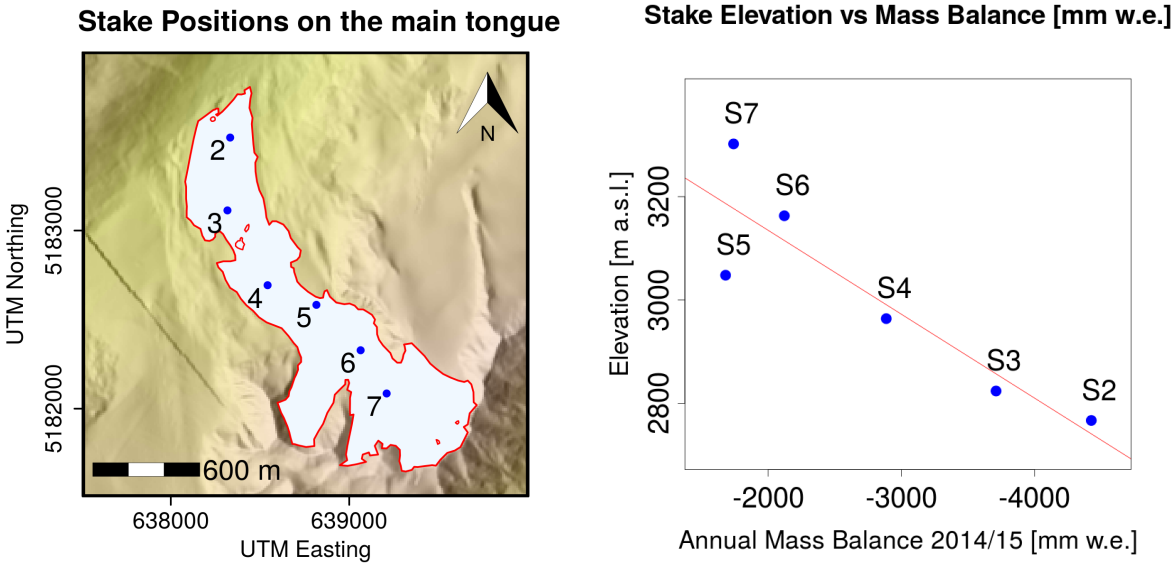

Figure 3.9: Left: Position of the six used ablation stakes along the main tongue of the glacier. Adjacent glaciated areas of Hochjochferner are not displayed. Glacier tongue shape updated 2013. **Right:** Stake elevation vs. measured annual mass balance. Linear regression in red.

1, see Tab. 3.2). Two stakes were intentionally placed in debris covered ice and will therefore not be used in this analysis, the residual six stakes were put along the flow line of the main tongue. As expected, a trend of decreasing ablation with increasing elevation can be seen (Fig. 3.9). Stake 5 is an exception, with less ablation than expected. The reason for this behaviour is not clear, as in the preceding hydrological year, ablation at Stake 5 seemed "in line" with the other stakes.

Two data points had to be estimated because they could not be safely accessed or were not visited for another reason (values coloured blue in Tab. 3.2). Especially stake 7, which is guarded by an icefall below, is sometimes not accessible. This was done by taking ablation measurements of similar elevation from nearby Hintereisferner, which is a very well-documented glacier located 4 km to the north-west. All measurements were converted to water equivalent by assuming a glacier ice density of 900 kg m^{-3}.

Table 3.2: Snow stake ablation data for the 2014/15 season. Stake 1 is located at the AWS site. Stake measurements are in [cm] of ice ablation. *NA*-values denote missing data. Blue values were estimated.

Stake	**Date**			**Total**	
	21/07/2015	**31/08/2015**	**30/09/2015**	**[cm]**	**[mm w.e.]**
1 (AWS)	-169	-238	-33	**-440**	**-3960**
2	-210	-251	-40	**-501**	**-4509**
3	-141	-247	-34	**-422**	**-3798**
4	-53	-248	-30	**-331**	**-2979**
5	0	-176	-22	**-198**	**-1782**
6	*NA*	-232	-8	**-240**	**-2160**
7	*NA*	*NA*	-200	**-200**	**-1800**

3.2.3 COSMO Data

The COSMO data used for this study consists of the daily 00 UTC forecast runs of COSMO-1. Before March 2016, COSMO-1 was tested pre-operationally. During this phase, it was subject to occasional changes in terms of model physics and domain extent. The forecast length for the 00 UTC run was changed a few times during that year, however, only the first 24 hours were taken of each run. The 00 UTC timestep consists of the analysis data from the ECMWF model, while each subsequent timestep consists of COSMO-1 forecast data. Also due to the testing phase, there were two gaps in the data, each covering not quite an entire day. These gaps - since they were rather small - were filled by using the same interpolation methods as for the AWS data, which are detailed in Chap. 3.2.1. The data was used at hourly timesteps.

Temperature and wind values were taken from the lowest atmospheric level of COSMO-1, which lies at 2 m above the ground level (a.g.l.) for temperature and at 10 m for wind data, respectively. Precipitation and radiation data was taken from the surface level. This difference was accounted for in the SNOWPACK configuration, as wind and temperature data height was set to 10 and 2 metres, respectively. The parameters taken from COSMO to run SNOWPACK were:

- Temperature data (air temperature and dew point temperature at 2m a.g.l.)
- Station air pressure
- Wind data (speed and direction at 10 m a.g.l.)
- Precipitation data
- Radiation data (diffuse and direct component of shortwave radiation as well as downwelling longwave radiation)

These parameters were extracted at the 6 closest grid points (see Fig. 3.11), the area between them covering the whole extent of Hochjochferner. Since COSMO-1's surface grid has a resolution of 1.1 x 1.1 km, the surface topography in the model does not exactly match the real topography, which leads to discrepancies in surface height between the model elevation and actual elevation. These elevation differences were accounted for by downscaling the COSMO data to the actual surface level. This is described in detail in Chap. 3.3.3.3.

Table 3.3: Grid Point metadata for the used COSMO-1 gridpoints. Coordinates in UTM Zone 32T, elevation refers to model topography. See also Fig. 3.11.

Grid Point	Easting	Northing	Elevation
Point 1	637651	5181982	2979 m a.s.l.
Point 2	637637	5183093	2951 m a.s.l.
Point 3	638765	5181996	3151 m a.s.l.
Point 4	638751	5183108	3063 m a.s.l.
Point 5	639880	5182010	3155 m a.s.l.
Point 6	639866	5183122	3141 m a.s.l.

3.2.4 Digital Elevation Model

As a digital elevation model (DEM), the official DEM of the county of Tyrol was used for the Austrian side of the border (updated 2010), while a DEM provided by the province of Bozen was used for the Italian side. Both were obtained via airborne

laserscans and are available at a resolution of 10 x 10 m. For the purpose of the study, the DEM'S were combined and a tile of 13 x 13 km covering the whole area of Hochjochferner and its vicinity was created. For the extrapolation calculations of the meteorological parameters, a tile of 2.5 x 2.5 km, covering the main tongue plus its surroundings, was used. Due to the elevation values in the DEM being from 2010, there were some differences between the recorded GPS height data from the stake measurements and the elevation of the same point in the DEM, because of ice ablation since 2010. However, as there is no more recent version available, all extrapolations and mass balance calculations were done with the elevation values from 2010. As the maximum difference is 35 m of elevation, the effect on the mass balance results should be negligible. For the actual GMB calculation on the main tongue, the shape and outline used by the University of Innsbruck's research team was taken, which was updated on 4th September 2013 (see Fig. 3.9).

3.3 Methods

3.3.1 Surface Energy Balance Calculation

As a first step to assess SNOWPACK's capabilities in this specific environment, surface energy balance (SEB) and ablation were modelled at the AWS site, where they could easily be validated with the data from the station. In this section, the calculation of the measured SEB fluxes to validate SNOWPACK's modeled SEB will be described. As a quick reminder, as specified in equation 2.5, the SEB of an open, flat snow or ice surface is given by (in units of [W m^{-2}]):

$$dE/dt = S_I + S_O + L_I + L_O + H_S + H_L + P + G. \tag{3.5}$$

G, the ground heat flux, represents the internal change of energy, e.g. by refreezing meltwater or heat advected from the underlying ground. Advection of meltwater or other energy sources is not possible in a one-dimensional model, and the ground heat flux in temperate glaciers (which is the case for Hochjochferner) is zero by definition. This is why, for both possible scenarios of either the glacier surface being directly exposed to the atmosphere or covered by snow, G is zero. It will therefore not be discussed further here. P, the flux of energy carried as sensible or latent heat by precipitation, is generally small and, since no liquid precipitation measurements are available, will also be neglected here. The incoming and reflected shortwave radiation S_I and S_O, as well as the incoming and outgoing longwave radiation L_I and L_O, were all measured by the weather station and therefore needed no further calculations. Which leaves the two turbulent fluxes remaining to close the energy budget: the sensible and the latent heat flux.

The sensible heat flux H_S is obtained with the use of a bulk transfer formulation, where fluxes are expressed in terms of the difference of a certain variable between its surface value and its value at a certain height z_{ref}:

$$H_S = \rho_a c_{p,a} C_H u(z_{ref})(T_a(z_{ref}) - T_S), \qquad [\text{W m}^{-2}] \quad (3.6)$$

where $c_{p,a}$ is the specific heat capacity of air, T_S is the surface temperature, $u(z_{ref})$ is the wind speed and $T_a(z_{ref})$ the air temperature, both at reference height z_{ref}, which is the height at which those values were measured (in this case 3 m above surface level). ρ_a is the air density, which is given by:

$$\rho_a = \frac{P}{R_d T_a}, \qquad [\text{kg m}^{-3}] \quad (3.7)$$

where P is the measured station air pressure in [Pa] and R_d is the specific gas constant for dry air. C_H in Equation 3.6 is the bulk transfer coefficient for heat. Over normal ground, where stable as well as unstable boundary layer conditions occur, bulk transfer coefficients are computed with the help of the surface layer similarity functions. These functions express how the actual wind speed, temperature and humidity profiles deviate from profiles observed under neutral conditions, and are generally solved iteratively. With the help of some simplifications however, an explicit expression for the transfer coefficients can be obtained in terms of the dimensionless bulk Richardson number:

$$Ri_B = \frac{g\zeta_{ref} T_a(z_{ref}) - T_S}{T_{mean} u(z_{ref})^2}, \quad (3.8)$$

where g is the gravitational acceleration, T_{mean} is the mean air temperature in the layer of depth ζ_{ref} and $u(z_{ref})$ is the wind speed at reference height z_{ref}. $Ri_B > 0$ for stable boundary layer conditions, which generally prevail over snow cover because T_S can not be $> 0°$ C. ζ_{ref} is the height of the layer over which the turbulent flux is calculated, and it is given by:

$$\zeta_{ref} = z_{ref} - HS, \qquad [\text{m}] \quad (3.9)$$

where HS is the actual snow height. Since $HS = 0$ during ablation season, $\zeta_{ref} = z_{ref}$ during that time. With the help of the bulk Richardson number, the last variable that is need to solve Eq. 3.6 explicitly, C_H, can be calculated. For $0 \leq Ri_B < \beta_1$, C_H can be expressed as follows:

$$C_H = \frac{\kappa^2 (1 - \beta_1 Ri_B)^2}{ln(\zeta_{ref}/z_0) ln(\zeta_{ref}/z_H)]}, \quad (3.10)$$

where κ is von Kármán's constant, β_1 is a similarity parameter (taken as $\beta_1 = 5$ (Garrat 1992)), z_0 is the momentum roughness length of the surface and z_H is the heat roughness length. z_0 is defined as the specific height z over the surface, where - under neutral conditions - the wind speed is zero.

The latent heat flux H_L is calculated by:

$$H_L = \rho_a L_{vi} C_q u(z_{ref})(q(z_{ref}) - q_S), \qquad [\text{W m}^{-2}] \quad (3.11)$$

where L_{vi} is the latent heat of sublimation for ice at 273.15 K, $q(z_{ref})$ is the specific humidity at reference height z_{ref}, and q_S is the specific humidity at the surface, which is usually taken as the specific humidity of air saturated with respect to ice at the prevailing surface temperature T_S. C_q is the bulk transfer coefficient for water vapor, which is, similar to C_H, given by:

$$C_q = \frac{\kappa^2(1 - \beta_1 Ri_B)^2}{ln(\zeta_{ref}/z_0)ln(\zeta_{ref}/z_q)]}, \quad (3.12)$$

where z_q is the roughness length for water vapor. As a snow cover is one of the smoothest land surface types encountered in nature, measurements indicate momentum roughness length values between $10^{-3} > z_0 > 10^{-4}$. Over glacier ice however, z_0 is a bit larger. In this study, for the ablation season, a value of $z_0 = 0.0044$ m was chosen, which is a realistic value over bare glacier ice (Armstrong and Brun 2008). z_H and z_q are generally assumed to be one order of magnitude smaller, thus $z_H = z_q = z_0 * 10^{-1}$ (Brutsaert 1975). Occasionally, ablating glaciers can develop larger roughness elements at their surface (e.g. glacier tables or crevasses). This can, in some cases, lead to roughness length numbers of up to $z_0 = 0.1$ m.

3.3.2 Glacier Mass Balance calculation

There are quite a few established ways of calculating the mass balance of a glacier. Which one is ultimately used, depends mostly on the available data. In this study, a combination of the Process-Model Method and the Glaciological Method will be used (Cuffey and Paterson 2010). The Process-Model Method uses meteorological models resolving the physical processes at work to determine surface mass exchanges. Melt and sublimation are determined by calculating certain meteorological key parameters and resolving the surface energy balance. Precipitation values are taken from weather models. Because of greatly varying micro- and mesoscale meteorological conditions, the GMB-model usually is calibrated for the glacier that it is used on. In this study, the model was calibrated on points where measured data was available. Then, using the Glaciological Method, two GMB's were calculated: One with the input of measured and extrapolated data, and one with the input of a numerical weather prediction model, interpolated between its closest grid points. Those two mass balances were compared to each other, and also to the manual reference mass balance routinely calculated by Rainer Prinz, a former member of the Ice and climate group of the University of Innsbruck, which is based on stake measurements and analysed terrestrial photographies. The models and approaches used in the process-model part are already described in

detail in other chapters, which is why this section will focus on elaborating the Glaciological Method.

For the Glaciological Method (Kaser et al. 2003), measurements of annual accumulated snow and ice mass gains and losses are acquired at a series of points on the glacier surface, usually along its flow line. At these points, the change in surface level is measured, usually with the help of drilled and frozen-in-place measurement stakes. The surface level changes are then multiplied with local density values. For glacier ice, a density value of 900 kgm^{-3} is assumed, while snow density is usually determined by digging snow pits and recording snow density profiles. This procedure yields the local mass balance at all measurement points. These values are subsequently taken as representative numbers for altitude bands spanning the width of the investigation area (see Fig. 3.10). The elevation range of these bands is determined by the total elevation difference of the glacier and the number of measurement points. Spatial interpolation over the whole glacier area then results in a glacier-wide total GMB, which is calculated via:

$$B = \sum_{i=1}^{n} b_i A_i, \qquad [\mathrm{kg}] \quad (3.13)$$

where n is the number of elevation bands used, and b and A are the local mass balance and area of elevation band i, respectively. B can then be converted to the mean specific

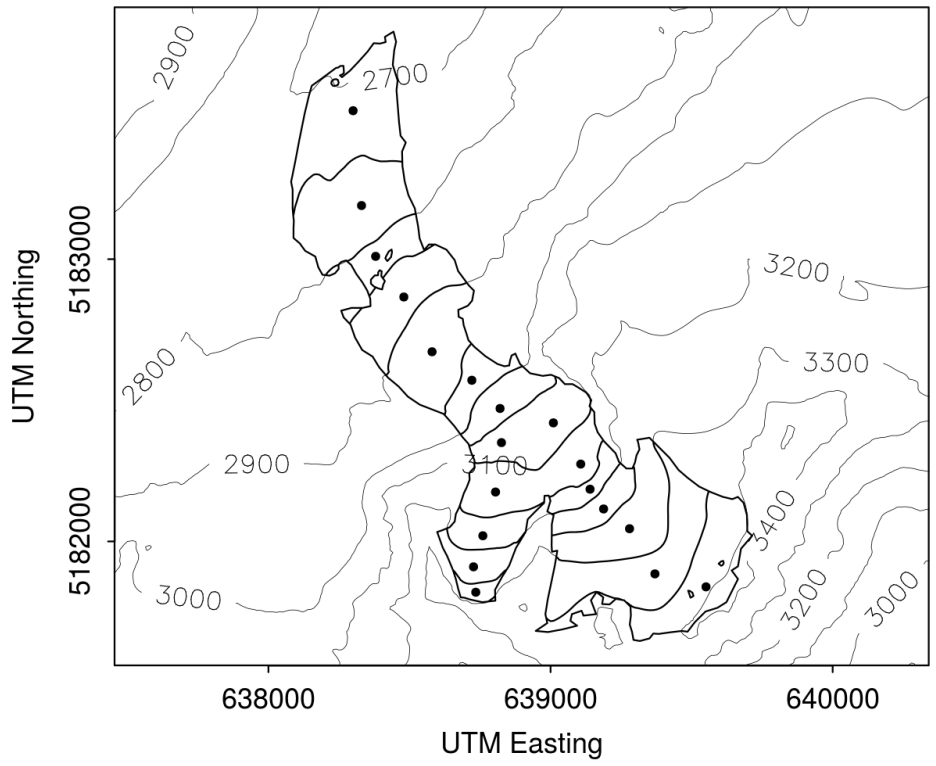

Figure 3.10: The used elevation bands (with a vertical spacing of 50 metres) and virtual measurement points for this study on Hochjochferner's main tongue.

mass balane $\bar{b}$ of the glacier via Eq. 2.4.

The main error source for this method lies in the problem of sampling. Since there is only a finite, usually rather small, number of measurement points available, these points have to be taken as a representative value for a whole zone, while there are different slope angles, orientations and terrain forms in each of these zones. A big part of the accuracy of the glaciological method comes down to the right choice of the measurement locations, which in turn requires experience and field work. For this study, the goal was to choose points that are representative for their elevation bands in respect to slope steepness and orientation, which was done via qualitative analysis of the used DEM.

3.3.3 SNOWPACK initialization and configuration

3.3.3.1 AWS Site

Since SNOWPACK simulations can be configured in a multitude of different ways, the settings, boundary conditions and initialization profiles used will be described here. SNOWPACK can be run with different meteorological input parameters. Naturally, all parameters were available from the AWS measurements. However, the goal was to eventually run the simulations also at other points, where only parameters that could reliably be extrapolated would be available. Thus, calibration runs at the AWS site were generally done with the same setup. The minimal input parameters required by SNOWPACK are:

- Air Tempereature (TA)
- Relative Humidity (RH)
- Wind Field (direction DW and velocity VW; strictly speaking, SNOWPACK can also be run just with VW, but since a reliable extrapolation algorithm was available, DW was used)
- Solid Precipitation (PSUM)
- Incoming Shortwave Radiation (ISWR)
- Incoming Longwave Radiation (ILWR)

These were also the parameters used for driving the simulation at the AWS site and the extrapolation sites. All the remaining, required parameters were parametrized by the model. Surface temperature as well as albedo were modelled at every timestep according to the current snowpack conditions and air temperature. From this, outgoing

shortwave radiation and outgoing longwave radiation can be calculated via Eq. 2.6 and Eq. 2.8, respectively.

An important factor for the calculation of turbulent fluxes is the measurement height of the meteorological parameters. In SNOWPACK, it can either be set to a fixed value above the ground level, or to a flexible value, where it stays at a constant absolute elevation (above sea level), and the distance between the measurements and the ground increases or decreases, depending on if a snow cover is building or melting. For avalanche modelling, because the station gets snowed in during winter and the distance between the sensors and the surface decreases, a flexible value is usually chosen, because it is important to accurately resolve surface energy fluxes during this period. However, as this study is focused on ablation modelling, the calculation of correct surface heat fluxes is much more important during ablation season. Additionally, with the melting glacier surface, a flexible measurement height would have led to unrealistically high values at the end of the ablation season (around 5 - 7 m above the surface, depending on the station), messing up surface energy flux calculations. And as the station is always standing directly on the glacier surface, even when it melts, a fixed measurement height value of 3 m a.g.l. was chosen.

There are several available boundary layer stability options with which SNOWPACK can be run. Normally, unstable boundary layer conditions are ignored when modelling the SEB of a seasonal snow cover because in practice, they do not occur during the winter months. For a glaciated surface, this is different however; since the snow/ice cover is present year-round, unstable conditions have to be included. Michlmayr et al. (2008) developed a boundary layer algorithm suited to the application over a glaciated surface, which was used for this study. They took the approach of Stearns and Weidner (1993) and modified it to account for the occasionally unstable conditions that can occur over glaciated surfaces in alpine climate regimes, mainly at times of intense heating during ablation periods. Additionally, as already described in Chap. 2.3, although a measured surface temperature was available, it was chosen to run the simulation with a Neumann boundary condition on top of the snowpack for the whole season, to allow for correct SEB calculation during melting periods and ensure comparability of the results.

SNOWPACK has the option to enable refreezing inside the snowpack, to simulate the nocturnal freezing of meltwater and formation of superimposed ice. For this study however, after some attempts, this option was found to be of not much use, since, due to low permeability of the underlying ice layers, most of the meltwater refroze at night, and total ablation amounts over the season were lowered by as much as 60%.

All model runs were done at a time resolution of 60 minutes. Because measurements were only available every full hour, and due to the nature of the processes inside the snow/ice body, choosing lower values would have only unnecessarily increased the

runtime of the simulations, while not significantly increasing accuracy.

While simulations in SNOWPACK are first executed on a flat field, the model is also capable of running slope simulations. As the incoming shortwave radiation (which depicts the biggest energy flux) is measured on a level sensor, but greatly varies depending on the angle and the orientation of a slope, this is a very important feature which has a big impact on available melt energy. Therefore, all simulations were first done on a flat field, and afterwards at the correct orientation and steepness of the slope at the respective locations (see Tab. 3.4).

Each run was started 14 days prior to the onset of the hydrological year (at 16th September 2014) to provide the model with some time to establish an internal balance. Initial glacier profiles, acting as a base for the simulation at the starting time, were defined. This was done by using the SNOWPACK-internal concept of .SNO-files, where each snow, ice or soil layer of a vertical profile, along with its defining physical parameters, can be specified. At the bottom, a soil layer with the properties and heat capacities of bare rock was created. On top of this, according to thickness measurements on Hochjochferner, 40 m of glacier ice were layered. The thickness of single layers was 1 m at the bedrock and got incrementally smaller towards the surface, where it was 2 cm. Since Hochjochferner is a temperate glacier, ice temperatures were assumed to be isothermal throughout the glacier at 273.15 K. According to Endres et al. (2009), the liquid water content of temperate glacier ice is 1.4 %. To be consistent with other mass balance studies, a glacier ice density of $\rho_i = 900\ kgm^{-3}$ was assumed. Therefore, the glacier ice was initialized with an ice to water to air content ratio of $\theta_i : \theta_w : \theta_a = 0.95 : 0.014 : 0.036$. In the snow profile, an albedo value for the glacier ice can be determined. Because of the very low albedo values encountered at the AWS site (see Chap. 4.1), an albedo of 0.16 was chosen for the ablation period, which is the same as the measured values.

3.3.3.2 Glacierwide Extrapolation

After testing the model at the AWS site, where all meteorological parameters were available for evaluating model performance, the next step was to run SNOWPACK at the positions of the 6 snow stakes along the flow line. For these runs, only ablation data was available as a measurement of SNOWPACK's performance. To get a modelled mass balance over the whole glacier, the following steps were taken:

- First, meteorological forcings for those six locations were created. This was done by spatially extrapolating the necessary meteorological parameters to run SNOWPACK on the 6 stake locations. As a starting point, the data collected by the AWS was used.

- At those locations, SNOWPACK was first run on a flat field and afterwards as a slope simulation (slope and azimuth values can be seen in Tab. 3.4). The results were verified with the measured ablation data.

- As the next step, 19 independent virtual mass balance points (VMBP) were created over the main tongue of the glacier, to divide it into sections with intervals of 50 m elevation. Again, meteorological parameters were extrapolated and SNOWPACK was run at each of those points in slope simulation mode.

- With the snow height and ablation data of these 19 points, the annual glacier mass balance was calculated according to Chap. 3.3.2.

Table 3.4: Slope angle and orientation for all snow stake locations and model simulations. For the slope angle, 0° represents a level surface, while for orientation, 0/360° denotes North.

Stake	**Slope angle [deg]**	**Orientation [deg]**
1 (AWS)	11.68	328.9
2	10.38	334.1
3	9.89	325.6
4	8.61	302.4
5	21.95	317.8
6	21.93	307.7
7	21.61	308.1

The spatial extrapolations from the AWS site to the stake locations and VMBP were done with MeteoIO, a library for handling meteorological data before passing it to an application, in this case SNOWPACK. MeteoIO can perform multiple inter- and extrapolation algorithms with varying degrees of complexity, depending on the meteorological parameter and the initial data. Because there was just one starting point available (the AWS), only methods that can also be extrapolated from one available measurement point could be used. For the extrapolations, the MeteoIO-intern concept of "virtual stations" was used, where the user can create virtual meteorological stations at given locations, and the meteorological forcing data for these exact locations is generated according to the given configurations. For all algorithms, a digital elevation model (DEM) needs to be provided. For details on the used DEM see Chap. 3.2.4. Below, the extrapolated parameters and the algorithms used will be described shortly. All algorithm names refer to the necessary parameter value used in the SNOWPACK configuration file (see App. A).

Atmospheric pressure was extrapolated by using the "STD_PRESS"-algorithm, which, if run with one AWS station, creates a standard atmosphere and calculates the

offset according to the current difference between standard atmosphere and measured atmospheric pressure. Air temperature was extrapolated by using a fixed vertical lapse rate. For this, according to Petersen and Pellicciotti (2011), a lapse rate of -0.0055 Km^{-1} was chosen, which should provide the best fit for the given circumstances. Relative humidity, as there was only one station to work with, was assumed constant over the whole glacier area. This is of course a possible error source, but since no part of the glacier is exposed to significantly more wind or solar radiation than another, and the absolute elevation range from its highest to its lowest point is rather small, this approach was deemed reasonable. The wind field was extrapolated by using the "LISTON_WIND"-algorithm, which calculates wind speed and direction by including the local curvature and slope of the surface. The method is described in detail by Liston and Elder (2006). Precipitation amount was extrapolated by using a flexible vertical gradient of 0.05 % per m, which, at 1000 mm annual precipitation, roughly translates to 0.5 mm m^{-1} (Schwarb 2000). Additionally, solid precipitation redistribution was modelled using the "PSUM_SNOW" algorithm. This distributes precipitation according to the wind field and the local curvature of the slope (Magnusson et al. 2011), which means it models snow distribution and erosion on a basic level. Incoming longwave radiation was extrapolated by using a fixed vertical lapse rate of -0.029 W m^{-1} (Marty et al. 2002). Finally, the incoming shortwave radiation was assumed constant over the whole glacier surface.

While there are a few potential error sources in these assumptions, it is the most sensible approach given that only one station is available as a starting point. In a case of 2 or more automated weather stations, more complex interpolation algorithms could be applied, but unfortunately this was not the case here. For the simulations with COSMO-data, other, more realistic interpolation algorithms could be used for some of the parameters (see Chap. 3.3.3.3).

For all SNOWPACK simulations, the same parameters and initial conditions as for the simulations at the AWS site (see Chap. 3.3.3.1) were used. All stake locations and virtual MB points were similarly initialized with a pre-existing snow profile containing 40 m of glacier ice in varying layers of thickness. However, a different albedo value was used on the main tongue. The AWS is located very close to the skiing area and shows unusually low albedo values both in winter and in summer (detailed discussion in Chap. 4.1). However, there is no evidence that the same values hold true for the main tongue further to the east. On photographs, the ice of the glacier where the AWS is located looks considerably darker than the main tongue, thus for the simulations on the main tongue, a "traditional" glacier ice albedo value of $\alpha = 0.3$ was assumed.

An example for an .INI-file used to configure a coupled MeteoIO & SNOWPACK-run can be found in Appendix A, an example .SNO-file to show how the virtual stations were set up in Appendix B.

3.3.3.3 SNOWPACK with COSMO-Data

In this section, an overview of the steps taken to run SNOWPACK with the available COSMO-1 data will be given.

- Meteorological forcing data was created by spatially interpolating COSMO-1-data to the locations of the AWS, the 6 mass balance stakes and the 19 virtual MB points
- SNOWPACK was run at all of these locations with the respective settings in slope simulation mode
- Modelling results at the AWS location and the 6 mass balance stake locations were compared to the measured AWS and ablation data to get an idea of the accuracy of COSMO
- A mass balance for the whole glacier was modelled using the same virtual mass balance points and elevation bands as with the extrapolated AWS data.

As already described in Chap. 3.2.3, data was extracted at the 6 closest grid points of COSMO-1 (Fig. 3.11). These grid points are all situated at different elevations, and to get meteorological forcing data at the stake locations as well as the virtual MB points, the data had to be spatially interpolated to the exact location and elevation of the points in question. This was again done via MeteoIO.

Atmospheric pressure was interpolated with the same algorithm as for AWS-data extrapolation, "STD_PRESS". Temperature data was first interpolated between the 6 grid points with an inverse distance weighting (IDW) algorithm. Each cell has its value determined by the weighted average of the whole data, with the weight being $1/r^2$, where r is the respective distance of the current cell to the contributing data points (here: grid points). The weights are being renormalized, so that the sum of the weights equals 1. Afterwards, the values were scaled to the true elevation by once again applying a lapse rate of -0.0055 Km^{-1} (Petersen and Pellicciotti 2011). Relative humidity was interpolated with the use of the "LISTON_RH"-algorithm, which is described in detail by Liston and Elder (2006). Since dew point temperature was part of the COSMO-data, it only had to be interpolated by once more using the IDW algorithm and scaling to the appropriate elevation, where it was converted to relative humidity. The wind field and precipitation data were interpolated by using the same algorithms as for AWS data, namely "LISTON_WIND" and "PSUM_SNOW", respectively, although with greater accuracy since there were now 6 data points available. Longwave radiation was interpolated by again using an IDW algorithm, and rescaled to the proper elevation with the same lapse rate as stated in Chap. 3.3.3.2, -0.029 W m^{-1} (Marty et al. 2002). Finally, shortwave radiation was calculated by using the "SW_RAD"-algorithm. At

each grid point, splitting coefficients (in diffuse and direct solar radiation) as well as an atmospheric losses factor were calculated, which were then interpolated to all other DEM cells using an IDW scheme. The potential solar radiation at each cell was rescaled using the splitting coefficients and atmospheric losses factor, as well as topographic shading of surrounding terrain, yielding the incoming shortwave radiation for a flat surface at each point in question.

For the SNOWPACK runs at the locations of the AWS, the mass balance stakes and the virtual MB points, the same configurations and snow profiles as described in Chap. 3.3.3.1 and 3.3.3.2 were used.

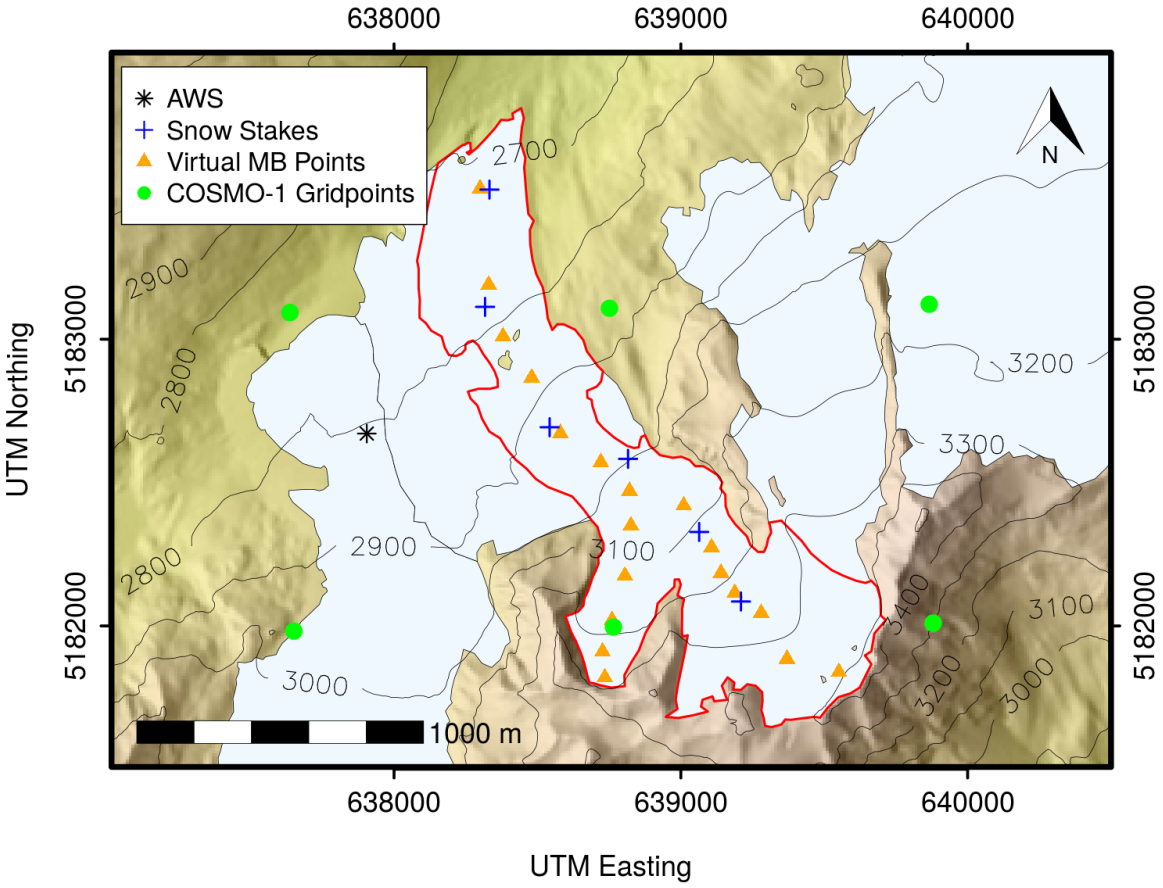

Figure 3.11: Overview of the HJF area, the main tongue outline in red, with the locations of the AWS (black star), the mass balance stakes (blue crosses), the virtual MB points (orange triangles) and the used COSMO-1 grid points (green dots).

4 Results and Discussion

4.1 Results at the AWS-Site

At the AWS site, first, the Surface Energy Balance (SEB) for the whole season was calculated and analysed. Details and equations are given in Chapter 3.3.1. The slope at the AWS-location has an angle of $\sim 11°$, with an azimuth of 329°, meaning it is oriented to the NW/NNW. All the components of the SEB are shown in Fig. 4.2.

Daily means of shortwave radiation (Fig. 4.2 a) show big differences, as expected. In winter, due to the orientation of the slope, the site only receives a minimal amount of solar radiation. The mean value of Incoming Shortwave Radiation (ISWR) during the winter months (December, January, February) is 82.8 Wm^{-2}, while the mean value during the summer months of June, July and August is 243.9 Wm^{-2} - nearly three times as much. For Outgoing or Reflected Shortwave Radiation (OSWR), while generally being lower than ISWR, values are rather similar during the winter and spring months, since the frequent snowfalls keep the albedo (see Eq. 2.6) rather high, in the range of 0.5 up to 0.9 (Fig. 4.1). As soon as the snow has melted however, the albedo goes down drastically. This can easily be verified when looking at the very low OSWR once the snow on the surface has melted, and the sudden increase in net shortwave radiation (see Eq. 2.7) at the start of July (Fig. 4.2a). Bare glacier ice has significantly lower albedo values than snow (a general assumption being 0.3). At this site however, AWS measurements indicate even lower numbers (see Fig. 4.1) during ablation season.

The mean albedo value from 2nd July to 3rd September 2015, which was the main ablation period in the 2014/15 season, was 0.16. Pictures of the AWS site (e.g. Fig. 3.4), as well as field reports, indicate very dirty ice in the area, which explains the low albedo values. Whether this is due to some sort of pollution because of the adjacent skiing area, or due to unknown reasons, cannot be determined at this point. According

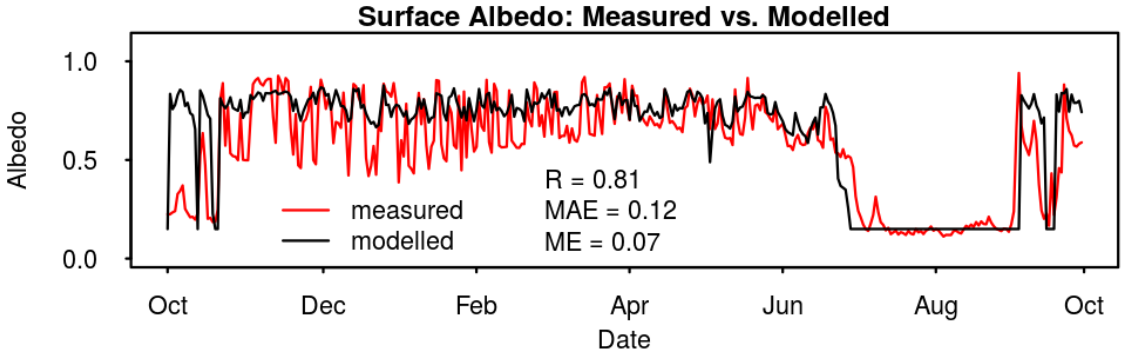

Figure 4.1: Comparison of measured (red) and modelled (black) albedo values.

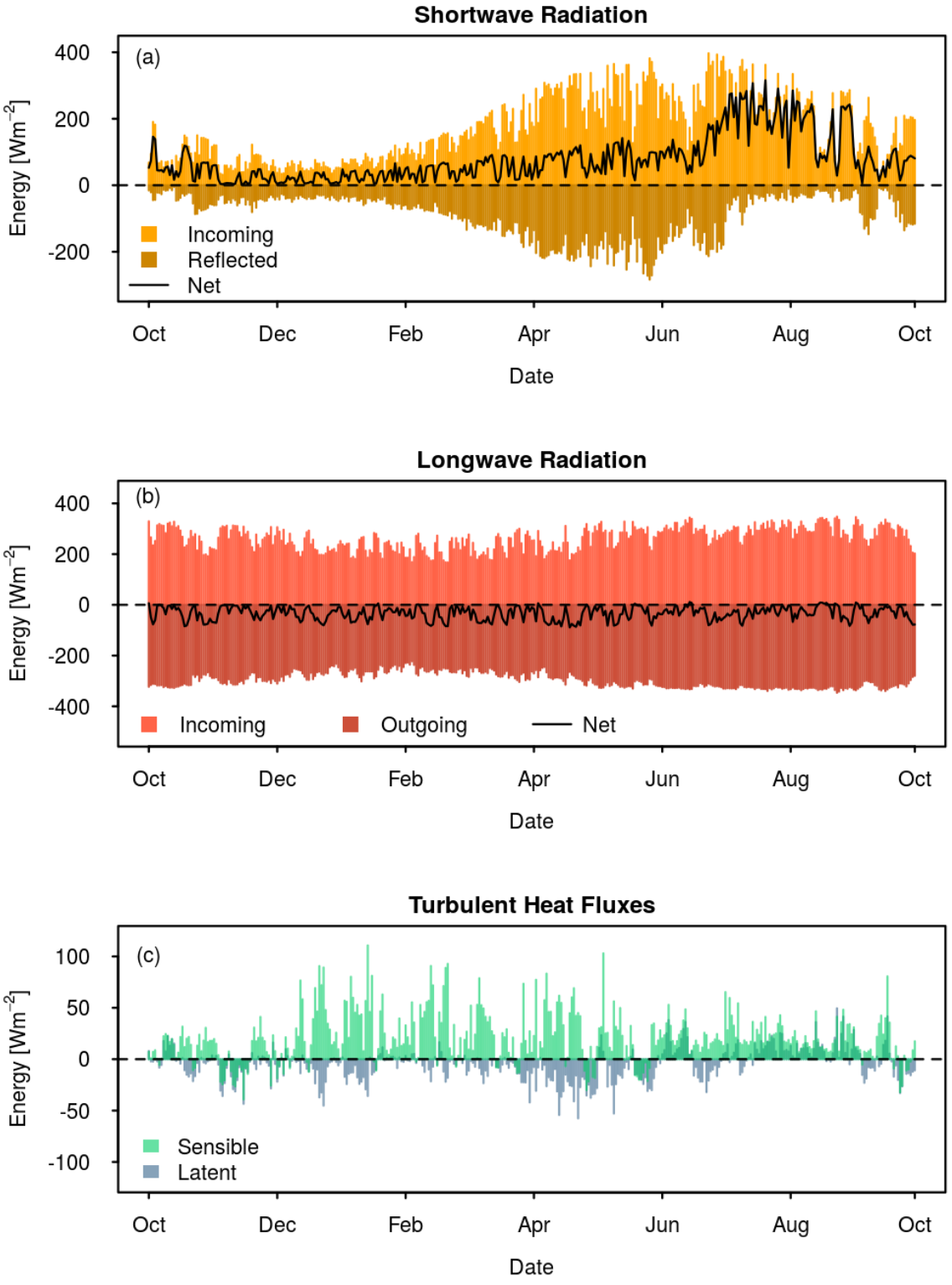

Figure 4.2: The Surface Energy Balance at the AWS. Daily means of **(a):** measured incoming, reflected and net shortwave radiation, **(b):** measured incoming, outgoing and net longwave radiation and **(c):** calculated sensible and latent heat flux.

to the measurements, a glacier ice albedo value of 0.16 was assumed for the simulations as well. Generally, the comparison between modelled and measured albedo shows a correlation of R = 0.81, with a mean absolute error (MAE) of 0.12 and a mean error (ME) of 0.07. Usually however, simulations run with SNOWPACK should be more accurate. When looking at the winter months, measured albedo also seems very low. Repetitively reaching values of 0.5 between December and February seems too low for that time of the year, especially given the altitude of the site. The snow either gets dirtier or wetter (both of which decrease albedo) a lot quicker than SNOWPACK simulates. The exact reason for this is not known, it is however very possible that the reasons are similar to the ones keeping the glacier ice albedo values as low as they are.

Shortwave radiation (Fig. 4.2 a) shows big annual fluctuations, as expected. The net shortwave radiation hovers just a little above zero during the winter months, but gets a lot bigger as soon as the snow is gone, and the low albedo of bare glacier ice takes effect.

Compared to shortwave radiation, longwave radiation only shows small fluctuations over the year (Fig. 4.2 b). Because it is proportional to the temperature of the emitting body (see Eq. 2.8), Incoming (ILWR) as well as Outgoing (OLWR) Longwave Radiation are of slightly less intensity in winter, due to lower temperatures of the surface as well as the atmosphere. Daily mean net longwave radiation is nearly always negative, with the exception of a few days mainly during summer.

The last two components of the SEB are the turbulent heat fluxes (Fig. 4.2 c). At high-elevation alpine sites in the midlatitudes, latent heat flux (H_L) is generally smaller than sensible heat flux (H_S). The sign, and also to some extent the magnitude, of H_S depend on the difference between air and surface temperature (see Eq. 3.6) - if $TA > TSS$, H_S is positive. Due to higher albedo values in winter, surface temperatures can be very low compared to the air temperature, which is why H_S is bigger during the winter and spring months. However, turbulent heat fluxes are also highly dependant on wind speed, which is why their magnitude cannot generally be tied to a season. As can be seen, H_S is mainly positive, as air temperature is usually higher than surface temperature over a glaciated surface. In comparison, the latent heat flux is mainly negative. This is due to the fact that for the air at the surface, saturation is assumed at all times, which is why specific humidity at the surface is most of the times higher than specific humidity of the overlying air. Since the relation between air temperature and its humidity storage capacity is exponential, in winter, when general air temperatures are colder, much less humidity is involved. In summer however, the difference in specific humidity is large enough for the latent heat flux to become positive.

In any case, as the magnitude of the turbulent heat fluxes is relatively small, and OLWR and ILWR are of the same magnitude but with different sign (so they balance each other out), net shortwave energy flux is the biggest contributor to the surface

energy balance. Quantitatively, shortwave net radiation contribution to the SEB at this site is 2.3 times bigger than longwave net radiation contribution, and 5 times bigger than turbulent heat flux net contribution.

In Fig. 4.3, the calculated and measured energy fluxes are compared to the ones modelled by SNOWPACK. The modelled net shortwave radiation (NSWR, Fig. 4.3 a) is almost zero during winter. This is explained by the albedo parametrization of SNOWPACK, as the modelled surface albedo is noticeably higher than measured values throughout the whole accumulation season (see Fig. 4.1). For the rest of the season, measured and modelled NSWR are in good agreement, as shown by a correlation of R = 0.95. The MAE is 20.6 Wm^{-2}, with a ME of -14.4 Wm^{-2} - this shows a clear negative bias of the modelled NSWR.

For the sensible heat flux (Fig. 4.3 b), the situation is the other way around: The agreement of the two graphs is better in winter than during the ablation season, where the measured H_S is noticeably lower than the modelled one. A likely reason for this is the fact that the OLWR values recorded by the station were at times too high. Per definition, the surface temperature of snow or ice can not be $> 0°\mathrm{C}$, however, values above that threshold were recorded by the OLWR sensor (this also explains the discrepancy between measured and modelled net longwave radiation in summer, see Fig. 4.3 a). The correlation R = 0.8 is lower than for NSWR, the MAE however is nearly the same (MAE = 20.5 Wm^{-2}). With a mean error of 19.1 Wm^{-2}, there clearly is a positive bias of the modelled H_S.

The latent heat flux (H_L, Fig. 4.3 c) looks similar to H_S, the general agreement is good but there is some discrepancy during summer. The reason is likely the same as for H_S, higher surface temperatures mean less moisture gradient, which in turn leads to lower H_L-values. The mean error is rather small compared to the MAE, which means there is no underlying systematic error. Finally, the comparison for the total SEB is plotted in Fig. 4.3 d. Because of the facts already discussed for NSWR, it is a similar picture for the SEB during winter, owing to the discrepancies between modelled and measured albedo values. For the rest of the year however, the agreement is quite good. The correlation is R = 0.92, and the mean absolute error 27.2 W m^{-2} with a ME of -8.9 W m^{-2}.

In Fig. 4.4, scatterplots of all the discussed SEB-components can be seen. Regarding ISWR and OSWR, as well as OLWR, modelled and measured values are in good agreement. Some scatter can be seen for ILWR (Fig. 4.4 b), which continues for net longwave radiation (NLWR, Fig. 4.4 c). Albedo shows two clusters at values around 0.2 and 0.8, which represent the ablation and accumulation season, respectively. The sensible heat flux (Fig. 4.4 c) shows very little scattering when it is low, but more for higher values, which is during the warm periods of the year. The plots for the latent heat flux as well as the total SEB show some clustering around 0.

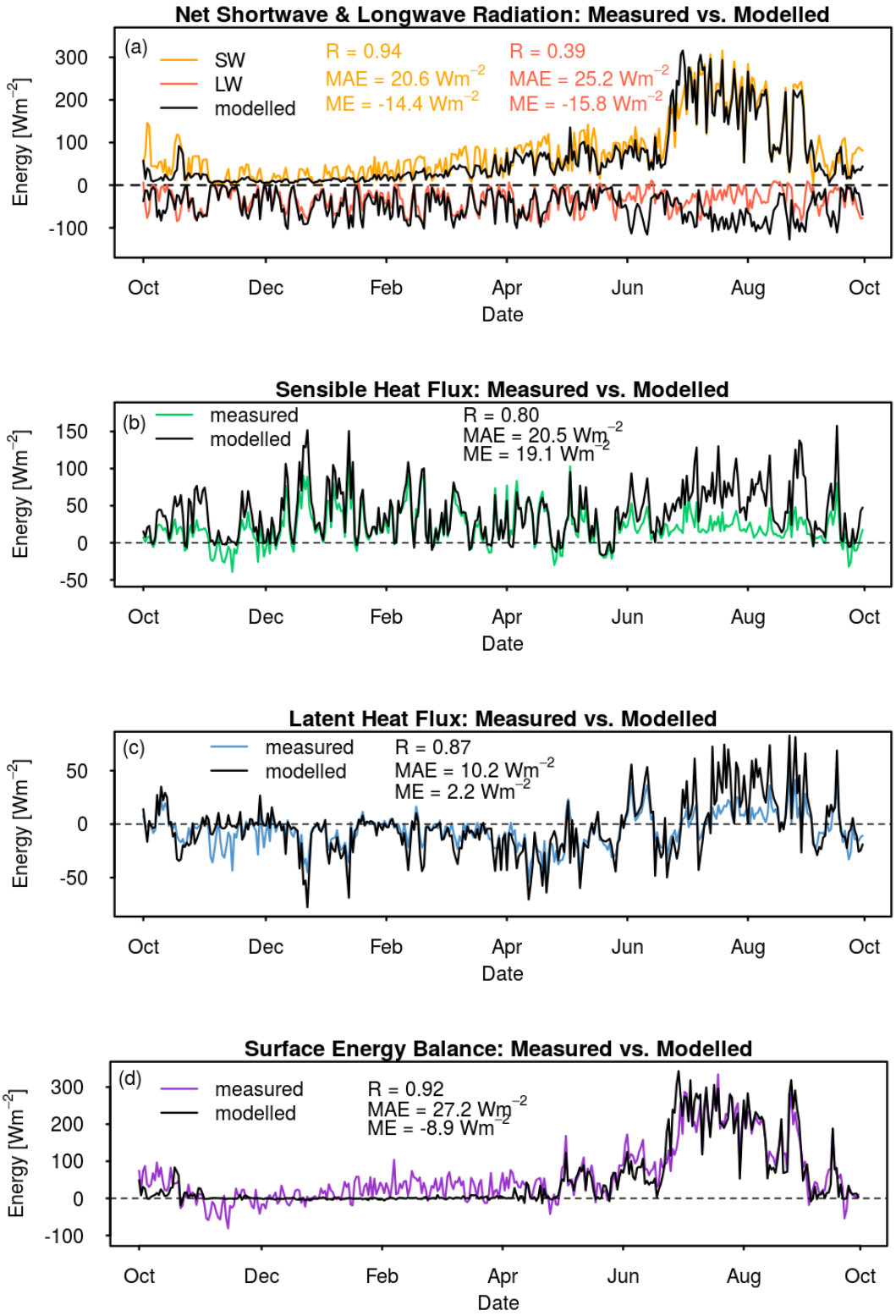

Figure 4.3: Comparison of the daily means of measured vs. modelled SEB: **(a):** Shortwave (yellow) and longwave (red) net radiation with their modelled counterpart (black). **(b):** Sensible Heat Flux, **(c):** Latent Heat Flux and **(d):** Total Surface Energy Balance.

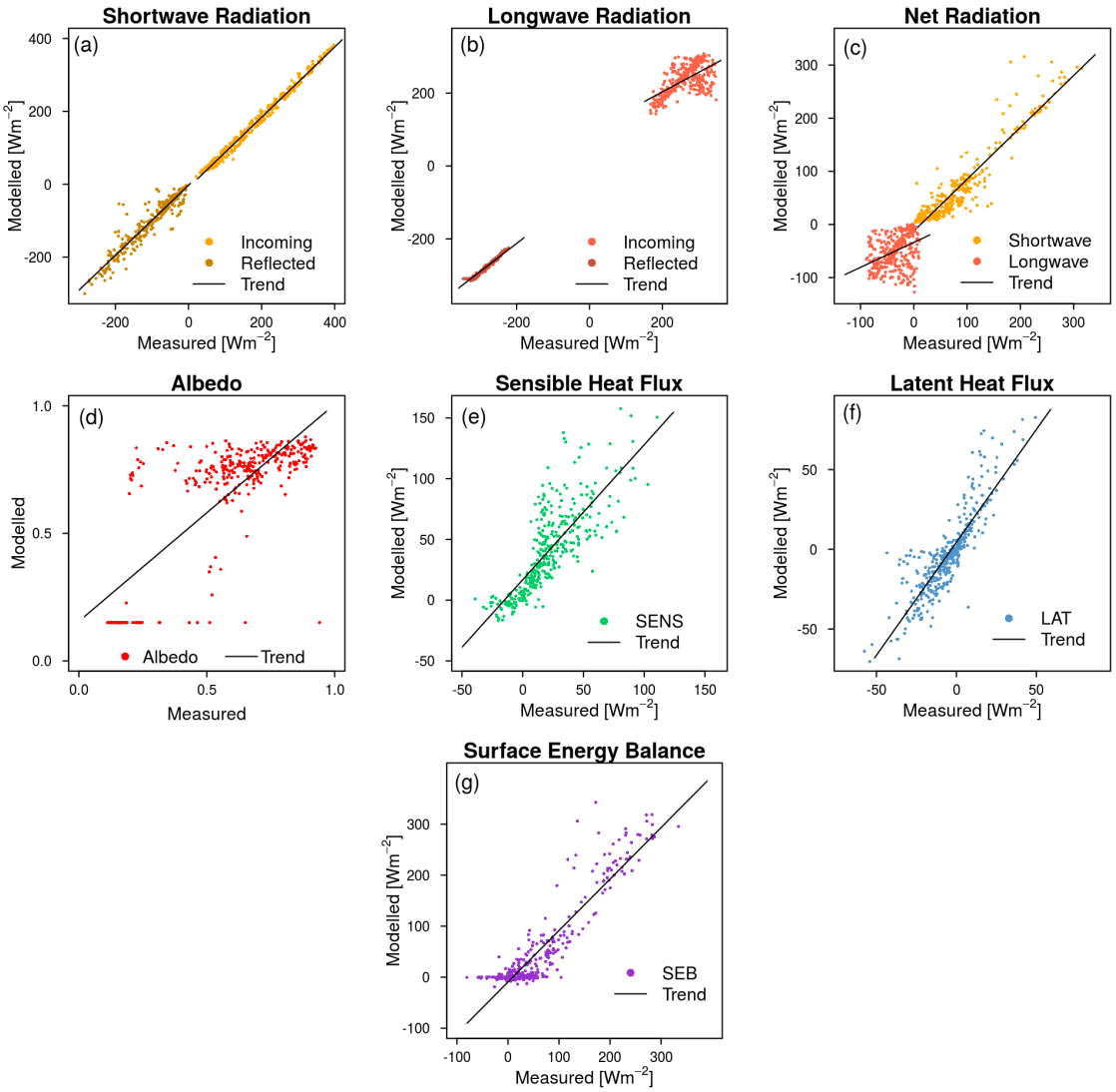

Figure 4.4: Scatterplots with linear regression lines for the components of the surface energy balance. Incoming and reflected shortwave radiation (a), incoming and reflected longwave radiation (b), net short- and longwave radiation (c), albedo (d), sensible heat flux (e), latent heat flux (f) and the total surface energy balance (g).

The modelled and measured snow and ice height are compared in Fig. 4.5. For comparability, measured snow heights were artificially raised by the exact ice thickness at the last hourly value in 2014 where $\alpha < 0.3$. This essentially adds the thickness of the modelled ice layer before the first lasting snowfall of the season to the snow height measurements, to make the modelled and measured values comparable. The black line shows the modelled combined snow and ice height, while the red line represents the measured values. The red dots denote ablation stake measurements at Stake 1 in direct vicinity of the AWS. During periods of ablation, where no snow height measurement was available, measured values were linearly interpolated. Those periods were defined as points where $\alpha < 0.3$, which essentially means before the 2nd and after the 3rd stake

measurement. The ablation date (the day where $\alpha < 0.3$ for the first time in a season) determined by the model was 29th June 2015, while according to measurements it was 2nd July 2015. Correlation between modelled and measured values is very high with a value of R = 0.99. The mean absolute error is 0.17 m, the mean error 0.01. Since the first stake measurement was done on 3rd October 2014, ablation values are calculated from that point onwards. The total measured ice ablation for the hydrological year 2014/15 was 4.4 m, while SNOWPACK determined a value of 4.56 m. For the calculation of the total mass balance in Tab. 4.1, as it has already been calculated manually using the snow stake data and terrestrial photographies, the same density values were applied to keep the numbers comparable.

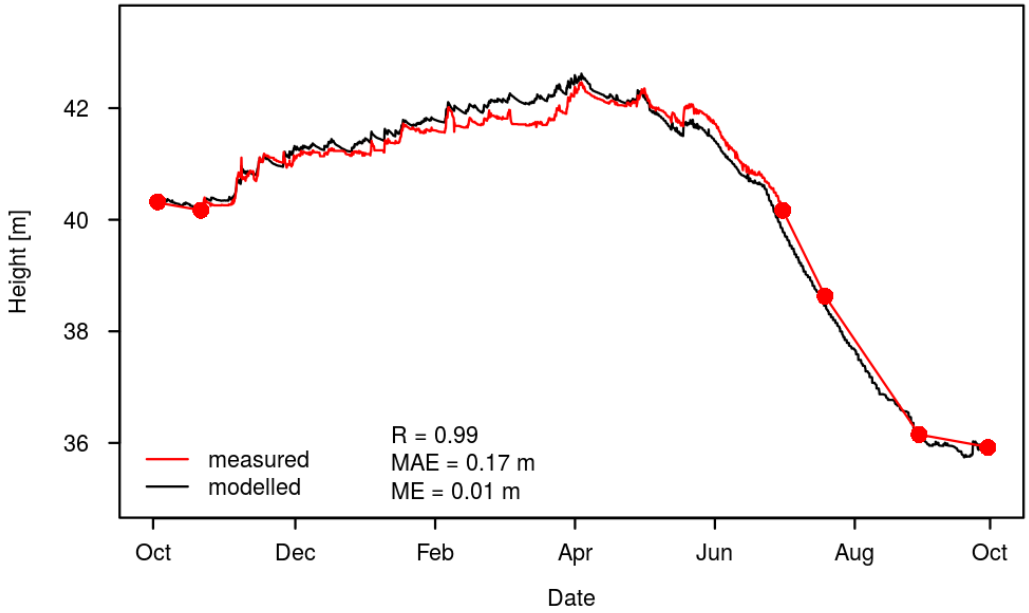

Figure 4.5: Comparison of measured (red) and modelled (black) snow/ice height. The red points mark ablation measurements taken at the AWS snow stake.

Table 4.1: Measured and modelled ablation values at the AWS snow stake. Ablation values shown are in [cm] since 03/10/2014. HS 30/09 represents the snow height that was measured on 30/09/2015 on top of the glacier ice. MB values are calculated assuming an ice density of 900 kgm^{-3} and a snow density of 460 kgm^{-3}.

	21/07	**31/08**	**30/09**	**Ablation [cm]**	**HS 30/09**	**MB [mm we]**
measured	-169	-238	-33	-440	23	-3854
modelled	-190	-225	-41	-456	17	-4026

Table 4.2: Summary of correlation and error values comparing calculated and modelled surface energy balance and snow height at the AWS site.

	R	MAE	ME
ALB	0.81	0.12	-0.07
Net SWR	0.94	20.6 Wm^{-2}	14.4 Wm^{-2}
Net LWR	0.39	25.2 Wm^{-2}	-15.8 Wm^{-2}
SENS	0.80	20.5 Wm^{-2}	-19.1 Wm^{-2}
LAT	0.87	10.2 Wm^{-2}	-2.2 Wm^{-2}
SEB	0.92	27.2 Wm^{-2}	8.9 Wm^{-2}
HS	0.99	0.17 m	-0.01 m

4.2 Glacierwide Extrapolation

For the glacierwide extrapolation, AWS data was extrapolated as described in Chap. 3.3.3.2, first to the 6 snow stake locations on the main tongue, and afterwards to 19 virtual mass balance points.

The SNOWPACK simulation's results for ablation at the 6 snow stakes can be seen in Fig. 4.6. The general agreement is quite good, however the ablation seems to be more accurately modelled in the lower regions of the glacier, while values start to diverge on the upper levels. As already discussed in Chap. 3.2.2, the measurement

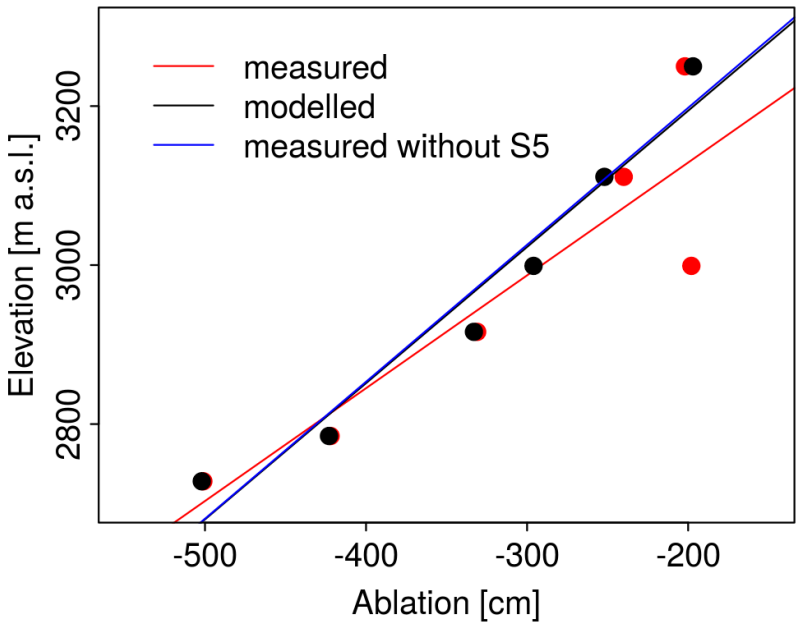

Figure 4.6: Stake elevation vs. ablation on Hochjochferner's main tongue. The red dots represent the measured ablation values, the black dots the modelled ones. Lines represent linear regressions of the data.

for Stake 5 is highly irregular for this season, which is why the measured and the modelled value differ for almost a meter. The red line displays the regression for all measured values, while, just for comparison, the blue line does the same but without the data of Stake 5. The black line represents the modelled ablation values, showing high correlation to the measured data with Stake 5 excluded.

In Fig. 4.7, all stakes are plotted separately for the ablation season from 21st July to the 30th September 2015. Again, red means measured, black means modelled values. Stakes 6 and 7 could not be measured at some of the dates, which is why there is missing data (see Chap. 3.2.2). Generally, again with the exception of Stake 5, the model performs quite well. Comparable values for 21st July are underestimated. This can probably be traced back to the earlier ablation date at the beginning of July, which means the model had a little head start concerning the ice melt. However, the gradient

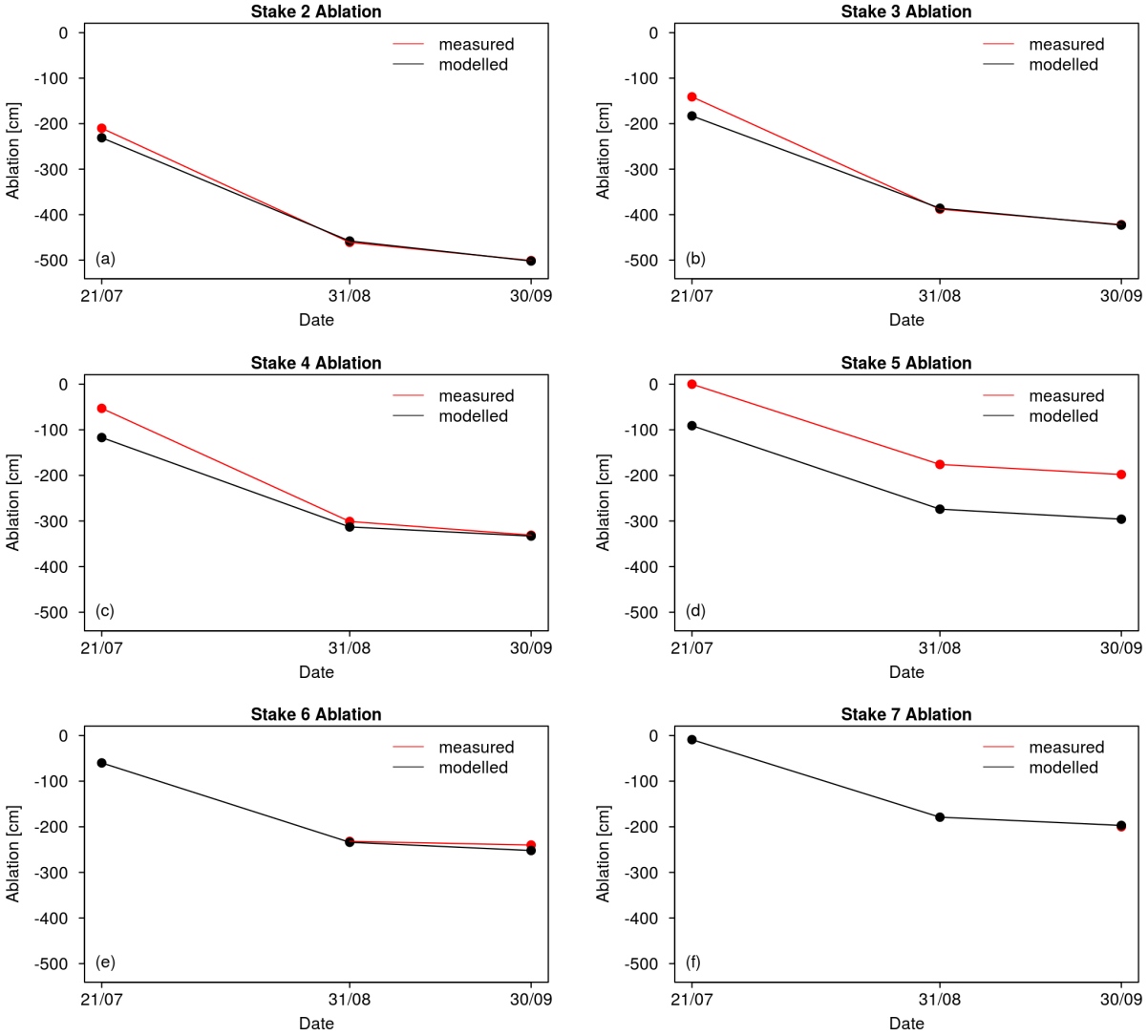

Figure 4.7: Individual comparison of ablation for each snow stake location. Measured values in red, modelled in black.

during the main ablation period between 21st July and 31st August also seems lower (Fig. 4.7 a, b and c), which means the model calculates a lower melt rate than the measurements suggest. This problem seems to vanish, or even revert (Fig. 4.7 e) during September, which leads to the conclusion that high-temperature, high-solar-radiation circumstances give SNOWPACK more trouble than cooler periods. Given the purpose that SNOWPACK was originally written for, the model is probably calibrated best for winter applications. Since the circumstances in spring are usually very different from winter, it can be tricky to calibrate the model in the right way. However, the differences are rather small.

The modelled mass balance over the whole glacier can be seen in Fig. 4.8. In general, values decrease (which means more ablation) with height along the main tongue. There is two zones where the gradient is reversed, precisely the 5th and the 10th zones counting from the bottom end, which represent the 2900 - 2950 m and the 3150 - 3200 m elevation bands, respectively. The reason for this is likely in the case of the lower zone, a significant change in terrain steepness (zone 5 is rather flat compared to the surrounding zones), and in the case of the upper zone, the terrain form. The upper el-

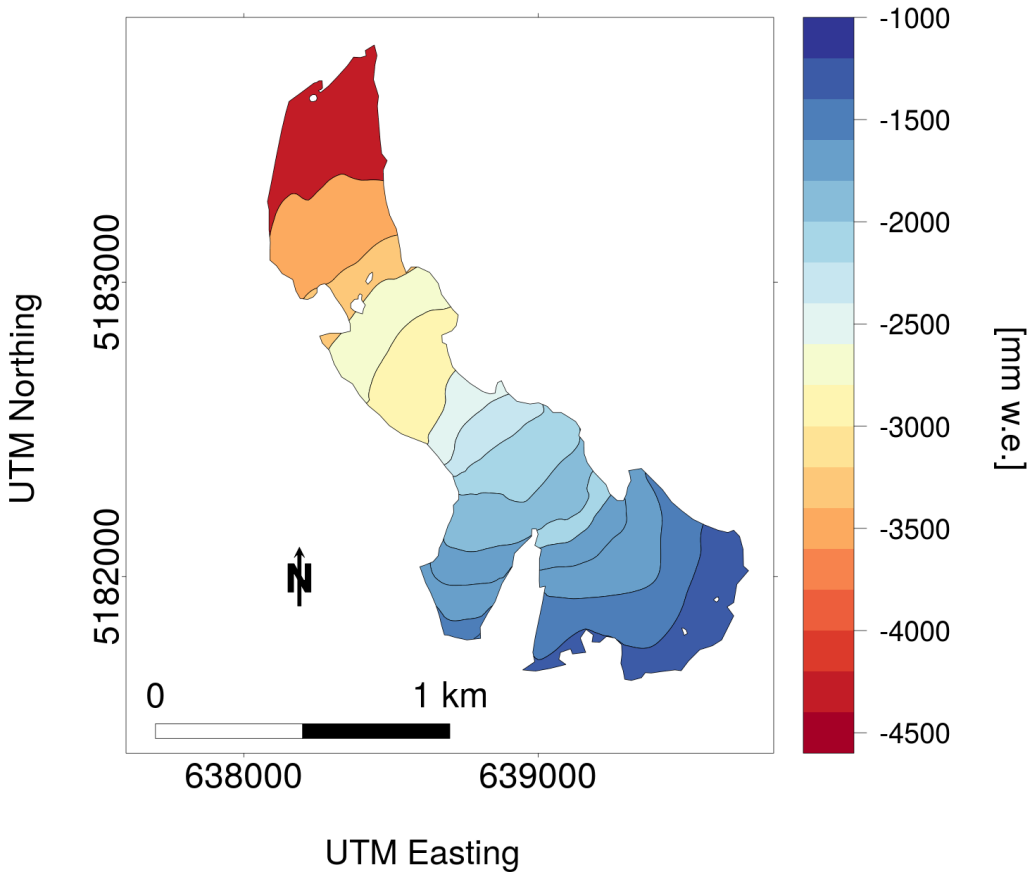

Figure 4.8: Modelled mass balance with SNOWPACK and extrapolated AWS data, for the main tongue of Hochjochferner.

evation band features convex terrain, which usually means less snow accumulation due to wind redistribution. This leads to an earlier ablation date and thus more total ablation. The western arm has a slightly less negative mass balance, as it is more northerly exposed and thus gets less direct solar radiation. In the modelled extrapolated mass balance, there is no accumulation zone on the whole glacier.

An annual mass balance for Hochjochferner for 2014/15 was already calculated by Rainer Prinz (former member of the University of Innsbruck's Ice and Climate group) using the stake measurements and the glaciological MB method (similar to this study). Additionally, he used terrestrial photos to identify small-scale accumulation spots and correct for faulty measurements, and created a manual mass balance where he combined the glaciological method with terrestrial photography analysis. In the calculated MB just with stake data, no accumulation zones are present on the glacier, while in the manual MB, with the help of terrestrial photos, some local spots were identified where a small amount of snow did not melt during the ablation period. These spots occur in areas that are very sheltered from the wind and where the terrain forms local depressions. Simulating them in a model could, if at all, only be done using a significantly higher resolution, coupled with a very high-resolution DEM, which was not available for this study. However, the results of the manual MB still show significantly

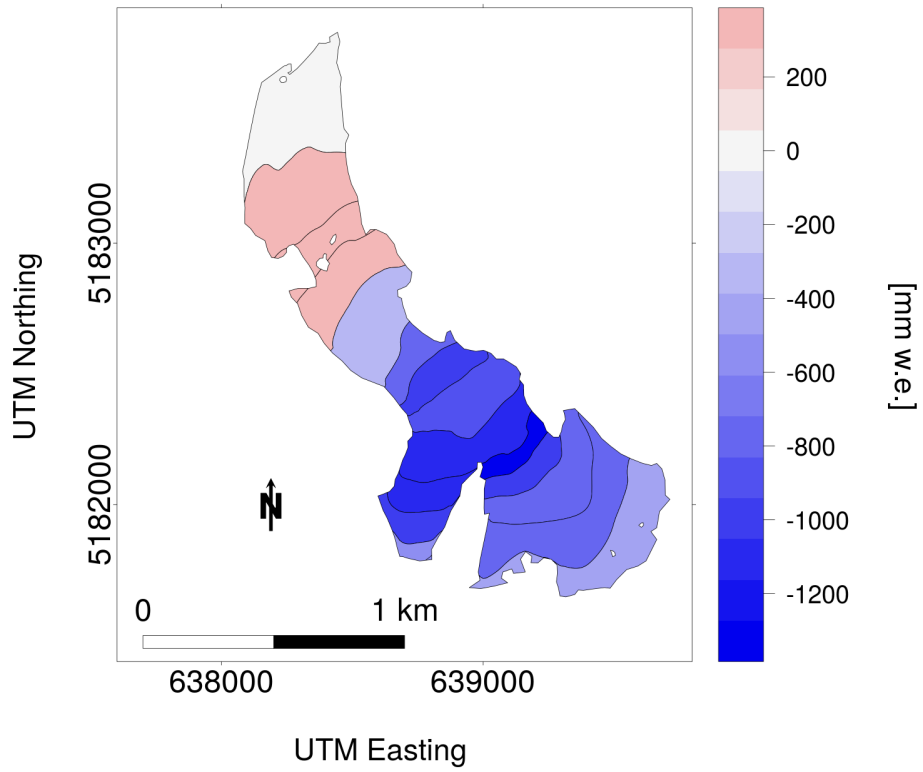

Figure 4.9: Difference between extrapolated and manual MB done by Rainer Prinz. Negative values mean less ablation in the manual MB and vice versa.

less ablation for the upper part of the glacier compared to the stake measurements, with the difference stemming from photography analysis.

In Fig. 4.9, the difference between the extrapolated MB done for this study, and the manual MB done by Prinz, is shown. As already stated, the manual MB resulted in significantly less ablation in the upper part of the glacier, hence the rather big difference in that part.

4.3 Results with COSMO-Data

The next and final step was calculating the mass balance with COSMO-1 forecast data. Data treatment and preprocessing methods to get meteorological forcing data, as well as model configurations are treated in Chap. 3.2.3 and 3.3.3.3, respectively. As a general overview as to how downscaled COSMO data compares to the measurements of the AWS, in Fig. 4.10 the temperature and solid precipitation data are shown for both COSMO and the AWS. The temperature data is in rather good agreement overall, although the downscaled COSMO-data systematically underestimates TA. Whether this is due to erroneous forecast data, or because the downscaling with a constant lapse rate is inaccurate, can not be determined. A combination of both reasons is likely. The correlation is R = 0.98 and the mean absolute error is 1.21 °C for the daily mean temperatures, with a ME of -0.95 °C.

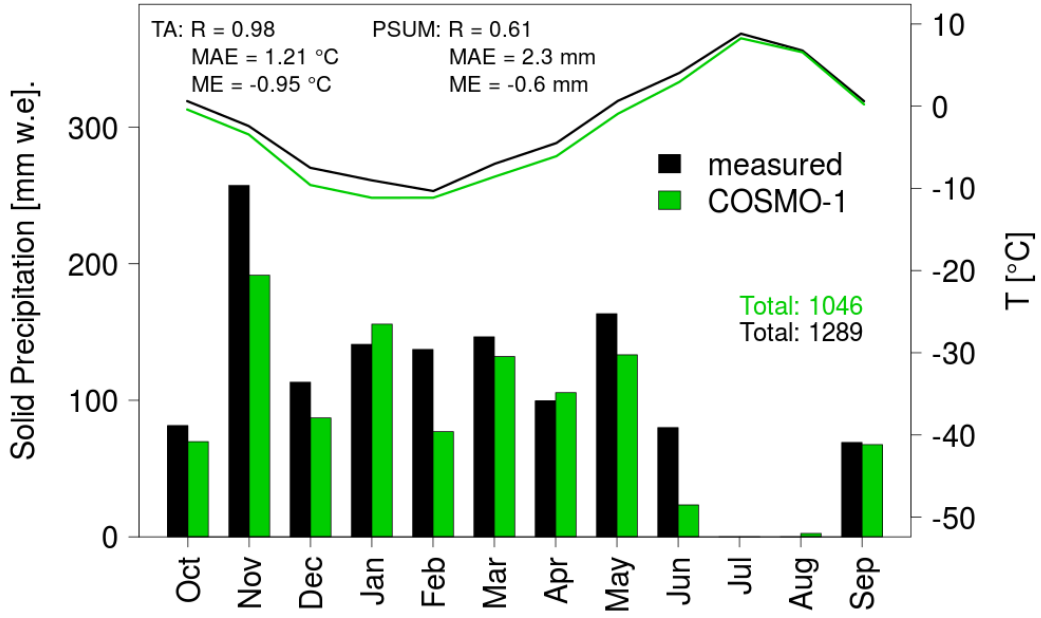

Figure 4.10: Measured AWS data compared to COSMO-data scaled down to AWS-location. Air temperature scale to the right, solid precipitation to the left. Modelled values in green, measured in black. Correlation and error values are based on daily means (TA) and daily sums (PSUM), respectively.

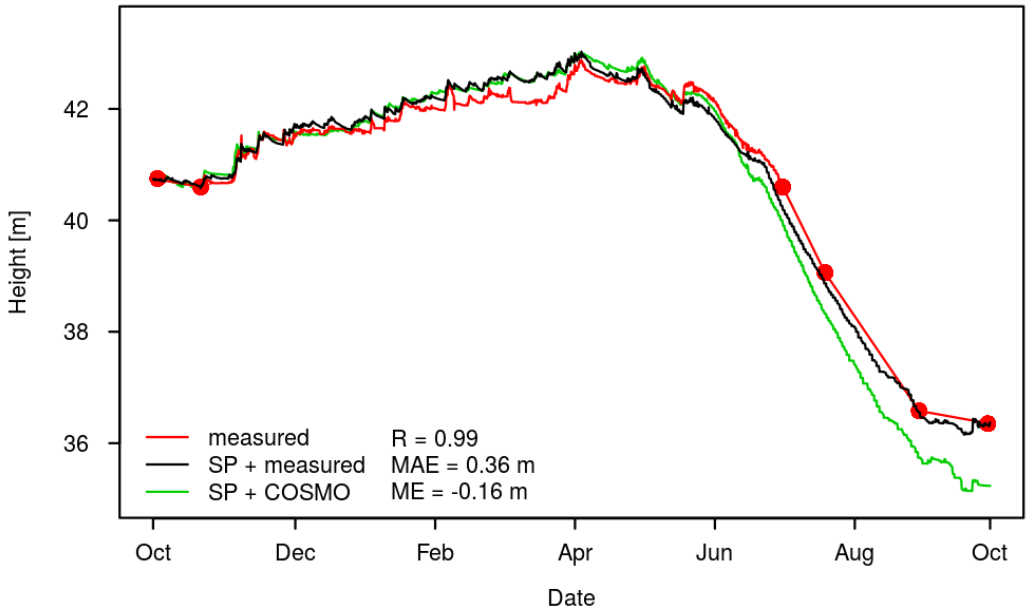

Figure 4.11: Comparison of snow height and ablation modelled with SNOWPACK at the AWS location. Measured data in red, SNOWPACK forced with measured data in black, SNOWPACK forced with COSMO-data in green.

Below the air temperature, monthly sums of solid precipitation are plotted. Surprisingly, the forecasted solid precipitation values by COSMO are actually lower than the measured values. This was not expected, since precipitation over mountainous terrain is traditionally overestimated by numerical weather prediction models. One possible explanation is that the vertical precipitation gradient used to rescale the forecasted precipitation amounts to the elevation of the AWS was too big. This would lead to a systematic underestimation of the values. However, snow height modelling shows that the modelled maximum snow height is in good agreement, and there is no sign of underestimation during accumulation season for the runs with COSMO-data (Fig. 4.11).

However, a constant density assumption of 90 kg m^{-3} was used for the conversion from measured new snow height to mm w.e. of solid precipitation, while SNOWPACK uses parametrized density values depending on meteorological variables (e.g. air temperature). This explains why, despite a difference of > 200 mm w.e., the snow heights still show a correlation value of $R = 0.99$. The mean absolute error is 0.36 m, however this is largely due to a rather big overestimation of ablation during summer for the runs with COSMO-data and not a systematic error, as is also proven by a ME of -0.16 m. Possible causes for this behaviour will be discussed in Chap. 4.4. One important thing to notice is the difference in the ablation date, which occurs a week earlier than measured for the COSMO-data-runs. Considering that the maximum snow height was actually modelled correctly, there have to be influences and processes that lead to over-

Table 4.3: Summary of correlation and error values comparing measured meteorological parameters with the results when using COSMO.

	R	MAE	ME
TA	0.98	1.21 °C	-0.95 °C
Solid PSUM	0.61	2.3 mm	-0.6 mm
HS	0.99	0.36 m	-0.16 m

estimated snow melt, which are probably the same as the ones leading to overestimated ice ablation. A summary of all errors discussed in this section can be found in Tab. 4.3.

The pattern of overestimated ablation for the runs with COSMO-data is also visible in Fig. 4.12, where the total ablation for 2014/15 at the six snow stake locations is plotted. The difference between modelled and measured values is about 30 - 50 cm for stakes at higher elevations, but adds up to almost 200 cm for the lowest part of the glacier tongue. The linear regressions also show a considerable difference in the ablation gradient with elevation between modelled and measured data. The measured vertical ablation gradient is steeper, meaning there is less variability in ablation values over the vertical extension of the glacier tongue. The nature of the differences leads to

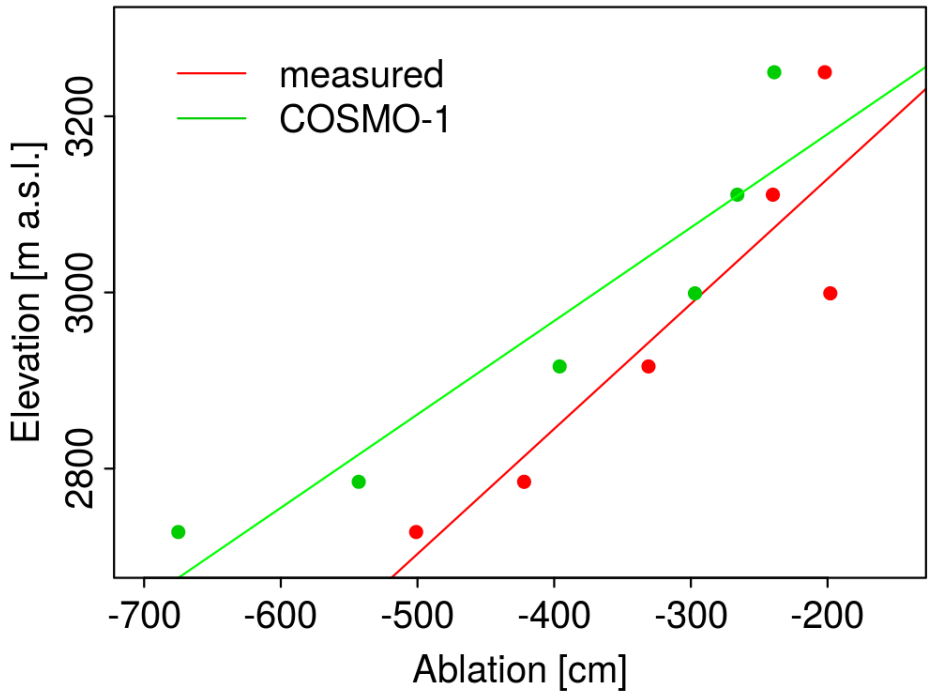

Figure 4.12: Stake elevation vs. ablation for measured (red) and modelled (green) data. Values are totals at the end of the season. Lines represent linear regression of the point data.

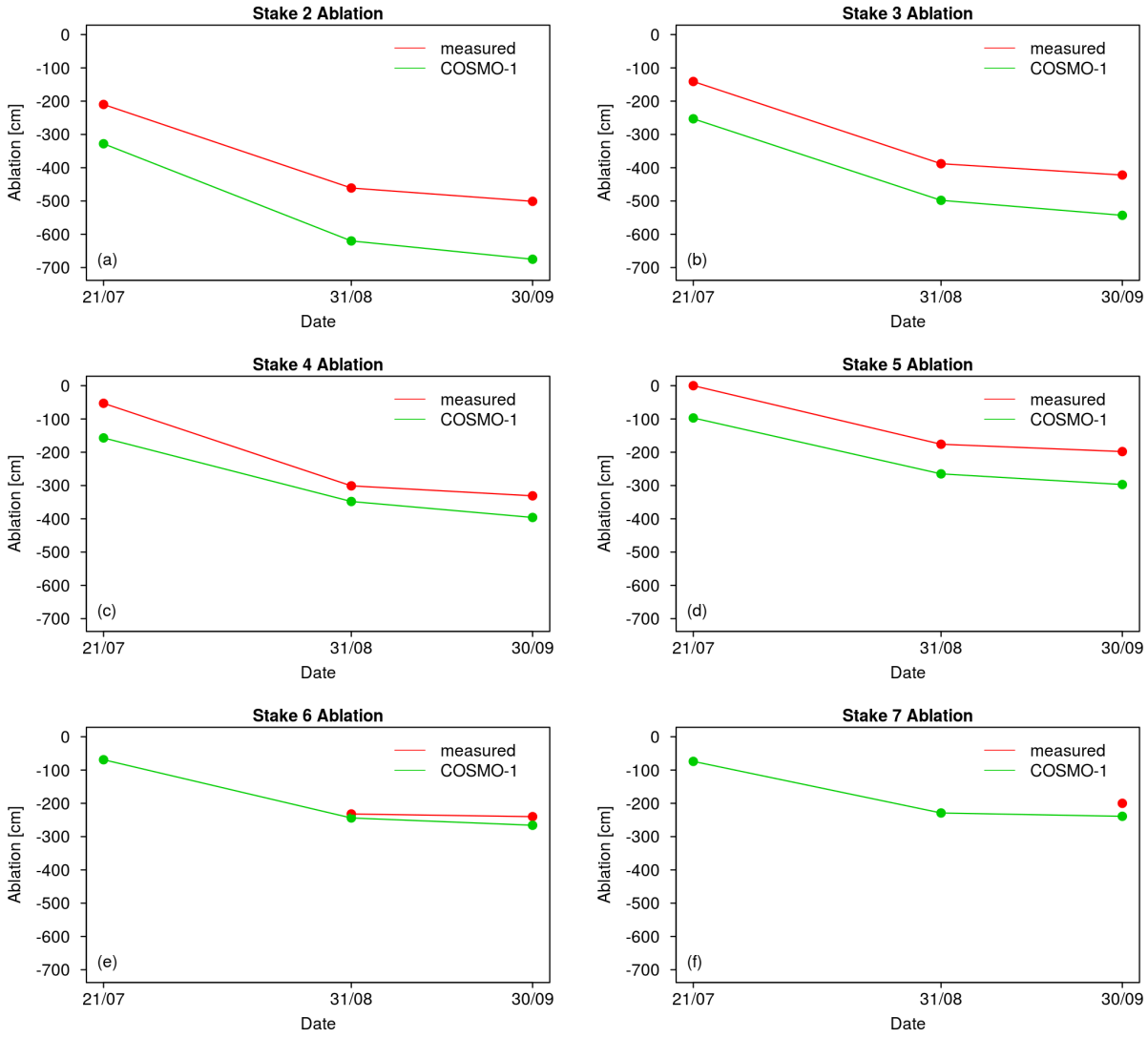

Figure 4.13: Individual comparison of ablation calculated with COSMO-data (green) to measured ablation (red) for each snow stake location.

the conclusion of an underlying systematic error, since there is a clearly recognizable and recurring pattern, and the error gets bigger with declining altitude. Again, possible causes will be discussed in the following section.

In Fig. 4.13, ablation values are plotted separately for each snow stake. Stake 5 has once more to be treated as an exception. In general, modelled ablation yields better results at greater altitudes. For the lowest snow stake location (Stake 2, Fig. 4.13 a), the simulation done with COSMO-data overestimates total ablation as well as melt rates over the whole season. As the error is already rather big on 21st July, this leads to the assumption that the ablation date is modelled too early in the runs with COSMO-data, which was also the case at the AWS-location. However, this can not be verified directly, as there are no stake measurements recorded earlier than for 21st July. When looking at the other stakes however, it can not be said that there is a general

overestimation of ablation rate. At Stake 3 for example (Fig. 4.13), which lies at approximately the same altitude as the AWS, the rate is the same as the measured one for the better part of the ablation season, and only in September it is overestimated. At Stake 4, ablation rates are even underestimated in the COSMO-data-runs for the main ablation season. Stakes 6 and 7 are missing crucial measured data points, which is why they are only of very limited use for comparison. One thing all stake simulations have in common, however, is the overestimation of the ablation rate during the last part of the season, in September.

As a last step, COSMO-data was downscaled to the 19 virtual mass balance points distributed over 17 elevation bands, and a modelled mass balance for the main tongue was created. The mass balance with COSMO-data can be seen in Fig. 4.14. The same pattern as in the mass balance modelled from AWS data is recognizable, with a generally declining mass loss with higher elevation. However, there are a few zones which do not strictly follow that pattern, e.g. again the 5th and the 10th zone counted from the bottom end of the glacier. The jump in total mass balance from the 3rd to the 4th zone is considerable, but so is the change of terrain; while the 3rd zone covers a convex, steep part of the glacier which often features bare ice and very little

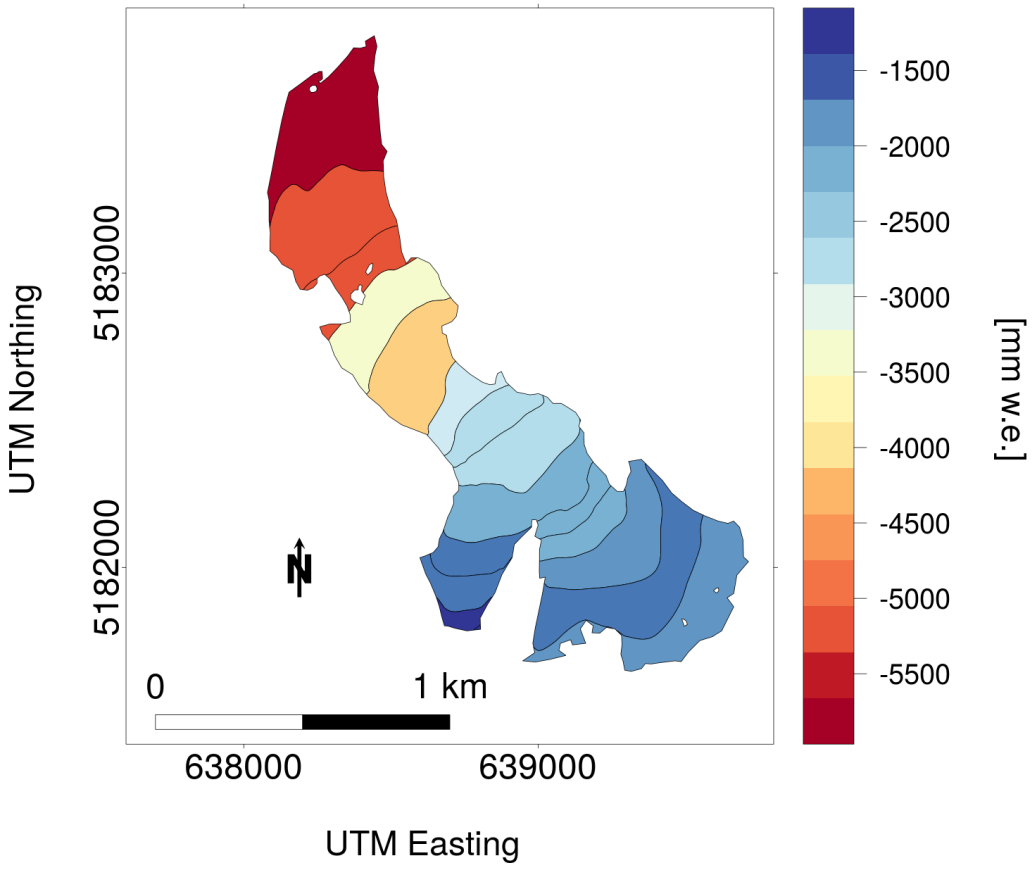

Figure 4.14: Modelled mass balance for the main tongue of Hochjochferner with COSMO-1 data.

snow accumulation, the fourth zone covers an area much less steep and exposed. An interesting point is that the range of total mass balance (the difference between the zone with the biggest and the zone with the smallest MB) is actually much bigger for the COSMO-data mass balance, with an ablation minimum of -1386 mm w.e. in the uppermost zone of the western arm and a maximum of -5667 mm w.e. in the lowest zone. The minimum for the MB modelled with AWS data is in the same range with -1316 mm w.e., the maximum however is only -4228 mm w.e.

In Fig. 4.15, the differences in modelled mass balances are plotted. To the left, the COSMO-forced MB is compared to the extrapolated MB. As can be seen, the difference in the upper parts of the glacier is generally in the range of 0 to 500 mm w.e. For the western tongue, the difference is even less than for the eastern tongue, the reason likely being the solar shading algorithm used to interpolate direct solar radiation. On the lower parts of the glacier however, there are considerable differences, with the maximum being 1439 mm w.e. in zone number 3 counted from the bottom. To the right, the MB modelled with COSMO-data is compared to the manual MB done by Rainer Prinz. The simulations forced with COSMO-data overestimate ablation over the whole glacier. While results are in better agreement in the upper part, the difference is still significant. The spectral patterns of the two comparisons are similar, but with a bias towards ablation overestimation for the COSMO-simulation when compared to the manual MB. In Tab. 4.4, a comparison of the mean specific mass balance for all used methods can be seen.

One thing to keep in mind is that there is no absolute "truth" to compare the modelled values to. While it is very likely that the manual MB is more accurate

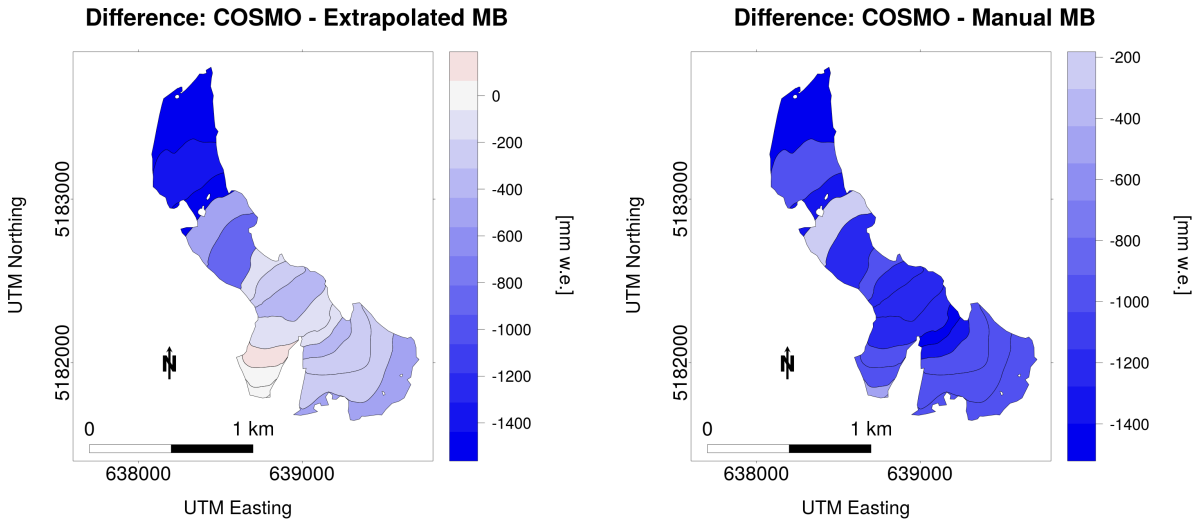

Figure 4.15: Differences between MB modelled with COSMO data and extrapolated AWS data (left) and MB modelled with COSMO data and the manual MB (right). Negative values mean overestimated ablation by the simulations using COSMO-data.

Table 4.4: Comparison of mean specific mass balance [kg m^{-2}] for the three different mass balance calculations.

Method	$\bar{b}$
Extrapolated MB	-2449 mm w.e.
COSMO-forced MB	-3070 mm w.e.
Manual MB (Prinz)	-2030 mm w.e.

and closer to reality than the extrapolated MB, it is still based on estimations from photographies and field measurements in an error-prone environment, and thus can not be taken as a definitive result based on which model performance can be accurately quantified.

4.4 Error Discussion

In this chapter, the errors along with their potential sources will be discussed. Although a general comparison of air temperature and winter snow height modelling at the AWS location looked quite promising, the mass balance modelling results, especially for the lower part of the glacier, show a considerable error when compared to the snow stake measurements and the available manual MB. Given that the results are more accurate when extrapolating the AWS-data using similar lapse rates and interpolation algorithms, the difference is most likely caused by the forcing data from COSMO. However, there is only one possibility to thoroughly check for the error sources, which is comparing the downscaled COSMO-data to the AWS measurements directly at the AWS location.

Since ablation is triggered by excess energy, in Fig. 4.16, the difference in daily means of total surface energy balance between the SNOWPACK-simulation run with AWS data and the run with COSMO data is plotted. The used formula was $SEB_{diff} =$

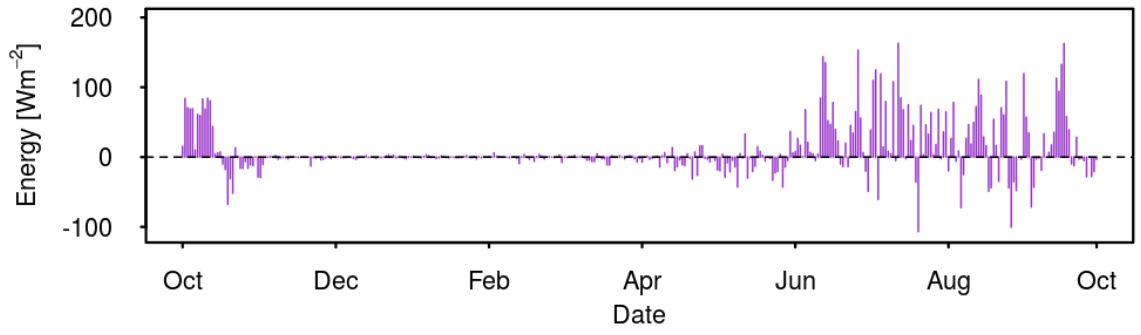

Figure 4.16: Difference in daily means of total surface energy balance between SNOWPACK runs with COSMO- and extrapolated AWS-data.

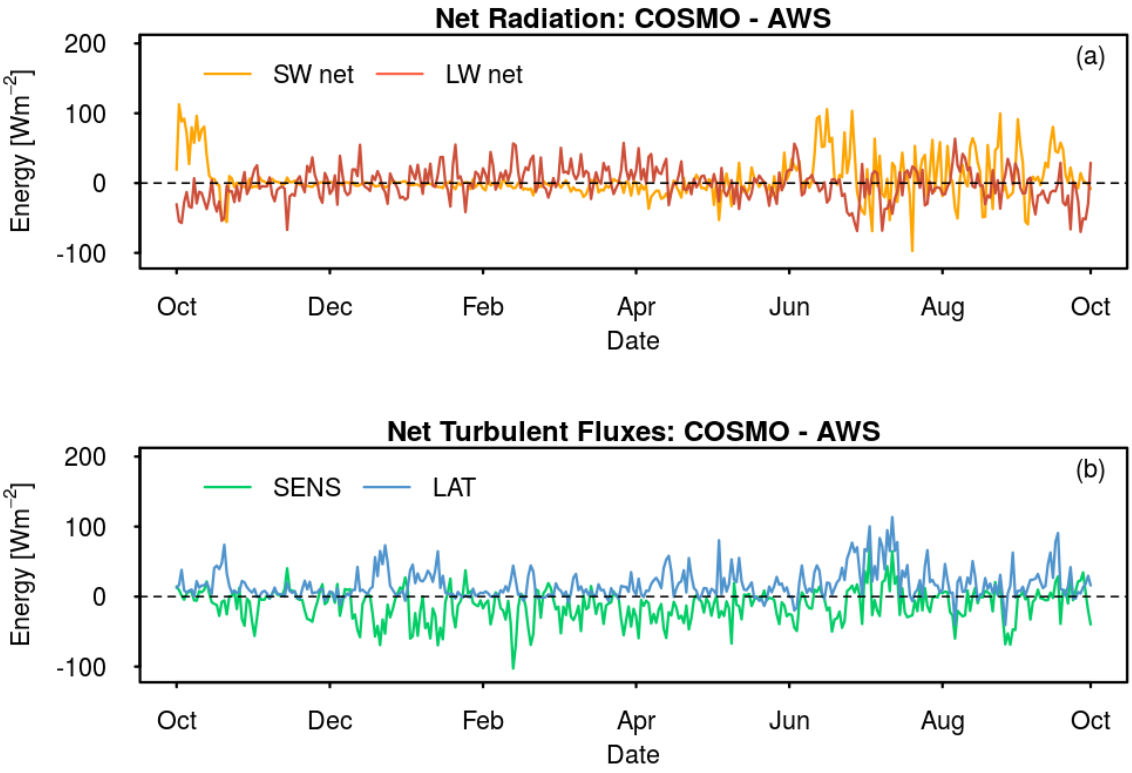

Figure 4.17: Difference in daily means of surface energy fluxes between simulations with COSMO- and with AWS-data: **(a):** Net shortwave (yellow) and net longwave (red) radiation. **(b):** Sensible (green) and latent (blue) heat flux.

$SEB_{COSMO} - SEB_{AWS}$, which means positive values point towards excess energy in the run with COSMO-data and vice versa. Since the simulations with COSMO-data result in more ablation, an energy surplus during at least the ablation season was expected, which is exactly what can be seen in Fig. 4.16. From October to the end of May, the difference is marginal, but starting with the beginning of June, it is significant. There are certain spikes that can be identified and traced back to already noticed anomalies, e.g. the first spike of excess energy in the middle/end of June, which very likely led to the early ablation date, as well as a spike in the middle of September, which explains the excess ablation at the end of the season for runs forced with COSMO data (see e.g. Fig. 4.11).

The difference in total surface energy balance is no big surprise, since the mass balance calculations already showed a difference as well. The interesting question is, however, which process(es) it is caused by. In Fig. 4.17, the differences for the single components of the SEB are plotted. The same interpretation as for Fig. 4.16 applies, with positive values showing excess energy in the simulations with COSMO data. Net shortwave radiation is pretty even for the accumulation season, but shows some differences during summer. Noticeable spikes can be seen in the middle of June,

as well as in the middle of September. However, from July to September, negative values can be seen too, which leads to a relatively balanced total difference. Longwave net radiation seems to balance out overall, and no significant anomalies can be seen during ablation season. The sensible heat flux is mainly negative, which means its impact would be towards less ablation. As the downscaled COSMO-data systematically underestimates measured air temperature at the AWS-location (either due to the data itself or due to a not quite realistic vertical temperature lapse rate, see Fig. 4.10), this was to be expected. During ablation season however, it swings back and forth between positive and negative values, thus having less impact than expected on ablation overestimation. The difference in latent heat flux is positive throughout the whole year, and especially during ablation season.

Tab. 4.5 shows the normalized sums of differences between the daily means of runs with COSMO- and AWS-data. Two periods were analysed, a period of heavy snow-melting from 1st to 30th June, and the main ablation period from 1st July to 30th September 2015. It is assumed that the total difference between the daily means of the surface energy balance is 1, with the other fluxes values being relative to the total. Important are the positive anomalies, since they lead to excess ablation. As can be seen, in June, the positive error is split between net shortwave radiation and latent heat flux. The reason for the high impact of solar radiation in June is that in the simulation with COSMO data, albedo is unusually low in periods of June, even going down to values of around 0.4, before jumping back up to 0.8. Thus, too much solar radiation is absorbed in the snowpack, causing faster melting and an earlier ablation date. For the ablation period however, the main contributor to the error is the latent heat flux by far.

Table 4.5: Normalized sum of the differences of the daily means of surface energy fluxes between simulations with COSMO- and with AWS-data for different time periods.

Date	SW net	LW net	SENS	LAT	SEB
01/06 - 30/06/2015	0.86	-0.18	-0.35	0.67	1
01/07 - 30/09/2015	0.39	-0.23	-0.18	1.01	1

According to Eq. 3.11, the main contributor to the magnitude of the latent heat flux is the difference in specific humidity between the boundary layer and the surface. For the latent heat flux to become positive, there needs to be more moisture present at measurement height than at the surface, where the air is assumed to be saturated at all time. If this is the case, latent energy is transferred to the snow and ice body through condensation or deposition. The phase change from water vapour to a liquid or solid state releases energy, which is absorbed by the glacier and thus available for melting. This can happen in two ways: Either air temperature is significantly higher

than surface temperature, or the relative humidity in the boundary layer is very high. Of course, also a combination of both is possible.

In Fig. 4.18, relative humidity measured by the AWS is plotted in blue, while relative humidity (RH) forecasted by COSMO is shown in black. The difference is significant, with measured RH going as low as 30 %, while the forecasted RH stays above 70 % for the whole season. Especially during summer, with higher air temperatures and thus more capacity to store moisture, the difference between measured and forecasted specific humidity becomes very big with RH-differences of up to 50 %. The MAE is 18.6 %, with a ME of 17.9 % - a distinct positive bias. Also, because of higher prevailing air temperatures, the effect is amplified at lower elevations, which explains the gradient between rather accurately modelled mass balance at higher elevations, and considerable errors in the lower part of the glacier. One possible reason for this significant difference is the absence of katabatic wind in the COSMO data. Katabatic wind systems often develop over glaciated surfaces, and they transport colder, drier air with less specific humidity downslope towards the lower end of the glacier tongue. The air is warmed up, resulting in a lower relative humidity. This effect would also lead to an increased error at lower elevations. Additionally, katabatic winds trigger mechanical turbulence in the boundary layer, which also lowers relative humidity. Another point is the cold bias of COSMO (see Fig. 4.10). COSMO is known for systematic underestimation of air temperature in mountainous regions, and lower air temperature at the same moisture content means a higher relative humidity.

Just for the sake of comparability, a simulation was run with the exact same COSMO-data, only relative humidity was substituted with measured RH from the AWS. The resulting difference plots can be seen in Fig. 4.19. As expected, the simulations with substituted RH-data yield more accurate MB results. For most of the glacier surface, the resulting ablation lies between the manually determined and the extrapolated MB-values, with the exception of zone 4, where simulations run with COSMO-data generally underestimate ablation. This was already pointed out earlier

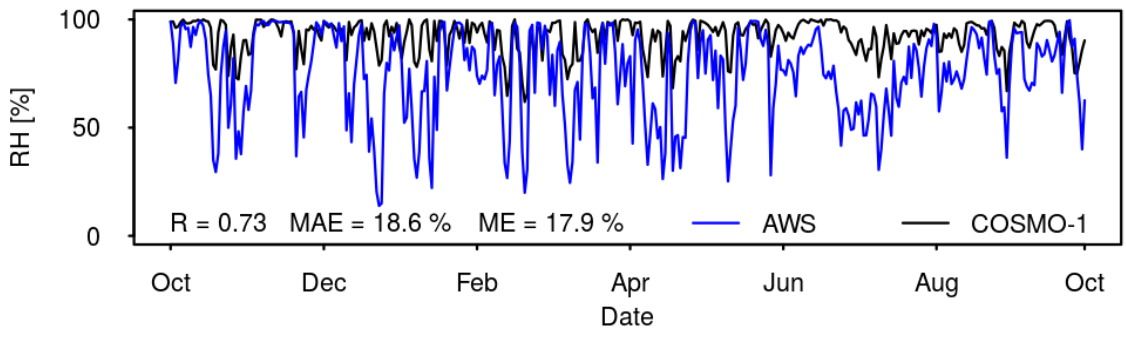

Figure 4.18: Comparison of measured relative humidity by the AWS (blue) and relative humidity forecasted by COSMO-1 (black)

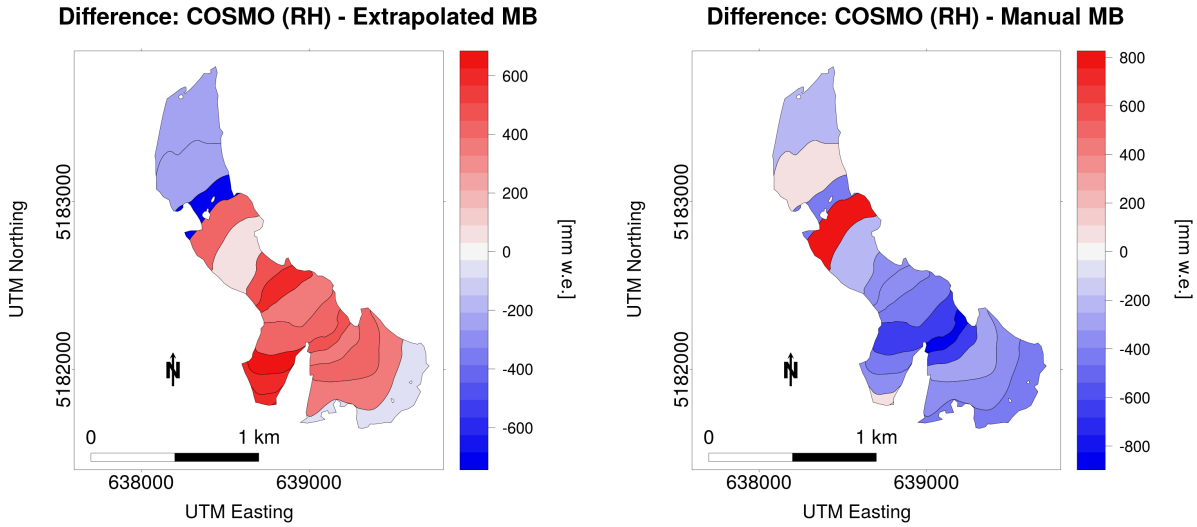

Figure 4.19: Results with COSMO-data but substituted measured RH-values at the AWS instead of forecasted RH values.

and can also be seen in Fig. 4.14. A possible explanation for this error is that maybe the virtual MB point was not set at an optimal location, resulting in an underestimated value for the whole zone.

In Tab. 4.6, the resulting mean specific mass balance (see Eq. 2.4) for Hochjochferner is compared for the different simulations and methods. If the manual MB is assumed to be closest to reality, COSMO-simulations with substituted RH-values yield the best results, with an error of 242 mm w.e. m^{-2} or 11.9 %. This translates to 26,9 cm of ice ablation overestimation.

Table 4.6: Mean specific mass balances for different simulations.

Source	Mean Specific MB $\bar{b}$ [mm w.e. m^{-2}]
Manual MB (Prinz)	-2030
SNOWPACK + AWS	-2449
SNOWPACK + COSMO-1	-3072
SNOWPACK + COSMO-1 (RH corrected)	-2272

Although the difference in relative humidity and the resulting latent heat flux overestimation is the main error source in the mass balance modelling, it is not the only one. As can be seen at the example of the month of June, just a few days of wrong albedo parametrization can already lead to considerable errors before the ablation season has even started. According to Tab. 4.5, albedo parametrization and the resulting absorbed shortwave radiation is the second biggest error source, followed by the sensible heat flux. An additional error source which can, under certain

circumstances, get important is the energy flux due to liquid precipitation, which also contributes energy to melting. It is ignored in the mass balance modelling at the AWS site and with extrapolations, but included in simulations forced with COSMO data.

For this study, the errors due to the individual sources and processes can somewhat be quantified, but in general, especially when working with forecast data from numerical weather prediction models, the error shares can often only be estimated.

5 Conclusion

The chosen approach to glacier mass balance modelling utilizes modern high-resolution technology and models that only became available in recent years due to increased computing capacities. As such, the theoretical capabilities of this model combination are definitely higher than standard bulk models neglecting important physical processes. However, more complex environments are always more prone to errors. SNOWPACK was not specifically made for modelling on a glaciated surface, and COSMO-1 as a project is still in its infancy. However, despite the experimental nature of the setup, good results can already be gained if one knows where to look for errors and what key parameters to look out for, as can be seen in Chap. 4.4.

The goal of this study was to find out whether the use of high-resolution models is viable for the application of modelling glacier mass balance with meteorological data from a numerical weather prediction model. To achieve this, at first the SNOWPACK model was tested locally at the site of the Automated Weather Station on Hochjochferner, to assess if it is capable of accurately modelling accumulation and ablation on a glacier over the course of a whole year. For this, SNOWPACK was run with data collected by the AWS. It was found that, although there were some discrepancies for single components of the surface energy balance, the results for the snow height and ablation model were accurate with a correlation of 0.99, a mean absolute error of 0.17 m and a mean error of 0.01 m.

As a second step, the meteorological forcing data was extrapolated over the whole glacier area with the help of MeteoIO. SNOWPACK was run at the six snow stake locations, and verified with the ablation measurements done there over the year. Again, the model performed quite well, although some differences could be seen in the ablation gradient. Afterwards, the forcing data was extrapolated to 19 virtual mass balance points, dividing the glacier tongue into 17 elevation bands, and SNOWPACK was run at those 19 points. When compared to the manual mass balance done by Rainer Prinz, the model performed well in the upper and lower regions of the glacier, but there were also zones with differences of up to -1200 mm w.e. at the medium elevation bands.

As a third step, SNOWPACK was run with forecast data provided by COSMO-1, again first at the AWS location, then at the six snow stake locations and finally at the 19 virtual mass balance points spread over the glacier surface. At the AWS location, model results were close to the measured data for all of the accumulation season. Still, ablation was overestimated by almost 2 m by the end of the season. At the snow stake locations, ablation overestimation of the same magnitude was found for the lower parts of the glacier. In the upper parts however, it was modelled rather accurately with end-of-season-differences of 0.3 - 0.5 m. When run at the 19 virtual mass balance points,

results were similar to the ones obtained with the use of extrapolated AWS data for the upper parts of the glacier, but with differences of up to 1.4 m for the lower parts. In total, the mean specific mass balance for the modelling forced with COSMO-data was -3070 mm w.e., while extrapolated AWS-data yielded -2449 mm w.e., compared to -2030 mm w.e. by the manual MB done by Rainer Prinz. This is a total difference of -1040 mm w.e., which means ablation was overestimated by an average of ∼1.15 m over the whole glacier area.

Michlmayr et al. (2008) came to an end result of a 0.3 m overestimation of mass loss using SNOWPACK for glacier mass balance modelling in their study. Even considering that, compared to their study (where measured meteorological data was used), a whole new data source, namely COSMO-1, was introduced, the resulting mean error of 1040 mm w.e. seems rather big. However, after some investigation, it turned out that COSMO-1 is systematically overestimating relative humidity at this location, which in turn leads to an overestimation of the latent heat flux and excess energy in the snowpack. Because of this, mass balance was modelled once more, but with measured instead of forecasted RH-values. This yielded the result of a mean specific mass balance of -2272 mm w.e. - which is a difference of 0.26 m when compared to the manual MB, and -0.20 m when compared to SNOWPACK modelling with AWS data.

Seeing that the error can be reduced to 0.26 m just by substituting measured values of relative humidity, there is clearly a possibility to model annual mass balances accurately with rather little effort. If both the relative humidity and albedo parametrization were optimized for application on glacier surfaces, this value could most likely be reduced to < 0.2 m.

In Chapter 1.3, three research questions were specified for this study.

- Can the measured ablation of Hochjochferner be recreated accurately with SNOWPACK and AWS data at a single point?

→ At the location of the AWS, annual ablation modelling with SNOWPACK and AWS data shows an accuracy of +0.16 m (4.56 m of ablation compared to the measured 4.4 m), which is an error of 3.6 %.

- Can the measured mass balance of Hochjochferner be recreated accurately using SNOWPACK and suitable extrapolation methods for the AWS data?

→ The mean specific mass balance obtained with the use of SNOWPACK and extrapolated AWS data is -2449 mm w.e., compared to -2030 mm w.e. yielded by the manual mass balance. This is a difference of 419 mm w.e., or an error of 20.6 %.

- How big is the difference between the measured mass balance of Hochjochferner and the modelled MB using COSMO data as an input and SNOWPACK to resolve the surface energy balance?

→ The difference in mean specific mass balance between the COSMO-forced model and the manual MB is 1040 mm w.e., which translates to an error of 51 %. However, with the substitution of one known erroneous parameter with measured values, the difference is reduced to 242 mm w.e., which translates to an error of 11.9 %.

In a high-alpine environment, where so many processes play a role in snow (re)distribution and energy transport, it will always be very difficult to accurately model a variable as complex and with such a multitude of influences as the glacier mass balance. However, especially in these regions, with their restricted access and harsh conditions, an estimate with an error of ± 1 m (or significantly less when correcting for relative humidity) is already better than an empirical estimation, or no value at all. Furthermore, in most of the published studies using SNOWPACK as a tool to simulate glacier mass balance, the mass loss is overestimated, which means that the real mass loss can be determined more accurately, as the overestimation is systematic and can thus be accounted for in the end result.

As such, with a bit of improvement on the already mentioned points of humidity and albedo parametrization, this model chain looks like a promising tool to assess glacier mass balances in areas where no measurements are available. For now, this holds only true for the alpine environment, but in theory can be expanded to every location where a high-resolution numerical weather prediction model is available. With the numerous configuration possibilities SNOWPACK provides, it is probably not the easiest to set up, but offers great capability to extend its use to (sub)tropical and polar latitudes as well.

An interesting idea for further research would certainly be the comparison to a large-scale global NWP model as ECMWF's IFS-HRES model, to quantify the improvement that a high-resolution model such as COSMO-1 really brings to the table. Also, a direct comparison for this exact glacier and timeframe, but with less complex models like the degree-day method or a bulk snowpack model, would help to quantify the improvement a high-resolution snowpack model is able to make. Additionally, the application of the model chain to a glacier with better on-site measurements over a longer time period would be desirable, since a single season can always be subject to anomalies or irregularities distorting the results. This would also allow the development of a simple corrective algorithm for relative humidity, should it prove to be a systematic problem over glaciated surfaces regardless of the site.

Bibliography

Armstrong, R., 2010: The glaciers of the Hindu Kush-Himalayan region: A summary of the science regarding glacier melt/retreat in the Himalayan, Hindi Kush, Karakoram, Pamir, and Tien Shan mountain ranges. Tech. rep., ICIMOD, Kathmandu, 20 pp.

Armstrong, R., and E. Brun, 2008: *Snow and Climate: Physical Processes, Surface ENergy Exchange and Modeling*. Cambridge University Press, Cambridge, United Kingdom, 222 pp.

Bartelt, P., and M. Lehning, 2002: A physical SNOWPACK model for the Swiss avalanche warning Part I: numerical model. *Cold Reg. Sci. Technol.*, **35**, 132–145, doi:doi:10.1016/S0165-232X(02)00074-5.

Bellaire, S., and B. Jamieson, 2013: Forecasting the formation of critical snow layers using a coupled snow cover and weather model. *Cold Reg. Sci. Technol.*, **94**, 37–44, doi:10.1016/j.coldregions.2013.06.007.

Bellaire, S., J. Jamieson, and C. Fierz, 2011: Forcing the snow-cover model SNOWPACK with forecasted weather data. *The Cryosphere*, **5**, 1115–1125, doi:10.5194/tc-5-1115-2011.

Brun, E., E. Martin, V. Simon, C. Gendre, and C. Coleou, 1989: An Energy and Mass Model of Snow Cover Suitable for Operational Avalanche Forecasting. *J. Glaciol.*, **35 (121)**, 333–342, doi:10.1017/S0022143000009254.

Brutsaert, W., 1975: The Roughness Length for Water Vapor, Sensible Heat, and Other Scalars. *J. Atmos. Sci.*, **32**, 2028–2031.

Buzzi, M., 2008: Challenges in operational numerical weather prediction at high resolutionin complex terrain. PhD dissertation, Swiss Federal Institute of Technoglogy (ETH) Zürich, 197 pp.

Cuffey, K., and W. Paterson, 2010: *The Physics of Glaciers*. Academic Press, Oxford, UK, 704 pp.

Dyurgerov, M., and M. Meier, 1997: Mass Balance of Mountain and Subpolar Glaciers: A New Global Assessment for 1961-1990. *Arctic and Alpine Research*, **29 (4)**, 4501–391, doi:10.2307/1551986.

Endres, A., T. Murray, A. Booth, and L. Wast, 2009: A new framework for estimating englacial water content and pore geometry using combined radar and seismic wave velocities. *Geophys. Res. Lett.*, **36 (4)**, L04 501, doi:10.1029/2008GL036876.

Fischer, A., B. Seiser, M. Stocker-Waldhuber, and J. Abermann, 2014: The Austrian Glacier Inventory 2006 (GI 3). Tech. rep., PANGAEA, Bremerhaven.

Garrat, J., 1992: *The Atmospheric Boundary Layer*. Cambridge University Press, Cambridge, United Kingdom.

Hock, R., 2003: Temperature index melt modelling in mountain areas. *J. Hydrol.*, **282**, 104–115, doi:10.1016/S0022-1694(03)00257-9.

Hoelzle, M., W. Haeberli, M. Dischl, and W. Peschke, 2003: Secular glacier mass balances derived from cumulative glacier length changes. *Global Planet. Change*, **36**, 295–306, doi:10.1016/S0921-8181(02)00223-0.

Horton, S., and B. Jamieson, 2016: Modelling hazardous surface hoar layers across western Canada with a coupled weather and snow cover model. *Cold Reg. Sci. Technol.*, **128**, 22–31, doi:10.1016/j.coldregions.2016.05.002.

Huss, M., A. Bauder, M. Funk, and R. Hock, 2008: Determination of the seasonal mass balance of four Alpine glaciers since 1865. *J. Geophys. Res.*, **113**, F01 015, doi:10.1029/2007JF000803.

Immerzeel, W., F. Pellicciotti, and M. Bierkens, 2013: Rising river flows throughout the twenty-first century in two Himalayan glacierized watersheds. *Nature Geoscience*, **6**, 742–745, doi:10.1038/NGEO1896.

Jiménez Cisneros, B., T. Oki, N. Arnell, G. Benito, J. Cogley, P. Döll, T. Jiang, and S. Mwakalila, 2014: *Freshwater resources. In: Climate Change 2014: Impacts, Adaptation, and Vulnerability. Part A: Global and Sectoral Aspects. Contribution of Working Group II to the Fifth Assessment Report of the Intergovernmental Panel on Climate Change [Field, C.B., V.R. Barros, D.J. Dokken, K.J. Mach, M.D. Mastrandrea, T.E. Bilir, M. Chatterjee, K.L. Ebi, Y.O. Estrada, R.C. Genova, B. Girma, E.S. Kissel, A.N. Levy, S. MacCracken, P.R. Mastrandrea, and L.L. White (eds.)]*. Cambridge University Press, Cambridge, United Kingdom and New York, NY, USA, 229-269 pp.

Kaser, G., A. Fountain, and P. Jansson, 2003: A manual for monitoring the mass balance of mountain glaciers. *Tech. Doc. in Hydrol.*, **59**, 137.

Klok, E., and J. Oerlemans, 2002: Model study of the spatial distribution of the energy and mass balance of Morteragschgletscher, Switzerland. *J. Glaciol.*, **48**, 505–518, doi: 10.3189/172756502781831133.

Kuhn, M., 2008: Methods of Assessing the Effects of Climatic Changes on Snow and Glacier Hydrology. *Snow and Glacier Hydrolog.*, **218**, 135–144.

Leclercq, P., and J. Oerlemans, 2012: Global and hemispheric temperature reconstruction from glacier length fluctuations. *Climate Dyn.*, **38**, 1065–1079, doi: 10.1007/s00382-011-1145-7.

Lehning, M., P. Bartelt, B. Brown, and C. Fierz, 2002a: A physical SNOWPACK model for the Swiss avalanche warning Part III: meteorological forcing, thin layer formation and evaluation. *Cold Reg. Sci. Technol.*, **35**, 169–184, doi:10.1016/S0165-232X(02) 00072-1.

Lehning, M., P. Bartelt, B. Brown, C. Fierz, and P. Satyawali, 2002b: A physical SNOWPACK model for the Swiss avalanche warning Part II: Snow microstructure. *Cold Reg. Sci. Technol.*, **35**, 147–167, doi:10.1016/S0165-232X(02)00074-5.

Lehning, M., P. Bartelt, B. Brown, T. Russi, U. Stoeckli, and M. Zimmerli, 1999: SNOWPACK model calculations for avalanche warning based upon a new network of weather and snow stations. *Cold Reg. Sci. Technol.*, **30**, 145–157, doi:10.1016/ S0165-232X(99)00022-1.

Liston, G., and K. Elder, 2006: A Meteorological Distribution System for High-Resolution Terrestrial Modeling (MicroMet). *J. Hydrometeor.*, **7**, 217–234, doi: 10.1175/JHM486.1.

Magnusson, J., D. Farinotti, T. Jonas, and M. Bavay, 2011: Quantitative evaluation of different hydrological modelling approaches in a partly glacierized Swiss watershed. *Hydrol. Process.*, **25 (13)**, 2071–2084, doi:10.1002/hyp.7958.

Marty, C., R. Philipona, C. Fröhlich, and A. Ohmura, 2002: Altitude dependence of surface radiation fluxes and cloud forcing in the alps: results from the alpine surface radiation budget network. *Theor. Appl. Climatol.*, **72 (3)**, 137–155, doi: 10.1007/s007040200019.

Marzeion, B., M. Hofer, A. Jarosch, G. Kaser, and T. Mölg, 2012: A minimal model for reconstructing interannual mass balance variability of glaciers in the European Alps. *The Cryosphere*, **6**, 71–84, doi:10.5194/tc-6-71-2012.

Mercanton, P., 1916: *Vermessungen am Rhonegletscher. Mensurations au glacier du Rhône. 1874 - 1915*. Gletscher-Kommission der Schweizerischen Naturforschenden Gesellschaft, 190 pp.

Michlmayr, G., M. Lehning, G. Koboltschnig, H. Holzmann, M. Zappa, R. Mott, and W. Schöner, 2008: Application of the Alpine 3D model for glacier mass balance and glacier runoff studies at Goldbergkees, Austria. *Hydrol. Process.*, **22**, 3941–3949, doi:10.1002/hyp.7102.

Moelg, T., N. Cullen, D. Hardy, G. Kaser, and L. Klok, 2008: Mass balance of a slope glacier on Kilimanjaro and its sensitivity to climate. *Int. J. Climatol.*, **28**, 881–892, doi:10.1002/joc.1589.

Morsier, G., Ed., 2015: *Developing a 1.1 km model setup at MeteoSwiss: Impact of changing the boundary conditions.*

Oerlemans, J., 2005: Extracting a Climate Signal from 169 Glacier Records. *Science*, **308**, 675–677, doi:10.1126/science.1107046.

Oerlemans, J., and J. Fortuin, 1992: Sensitivity of Glaciers and Small Ice Caps to Greenhouse Warming. *Science*, **6**, 115–117, doi:10.1126/science.258.5079.115.

Oerlemans, J., and N. Hoogendoorn, 1989: Mass-Balance gradients and climatic change. *J. Glaciol.*, **35**, 399–405, doi:10.1017/S0022143000009333.

Ohmura, A., 2001: Physical basis for the temperature-based melt-index method. *J. Appl. Meteor.*, **40**, 753–761, doi:10.1175/1520-0450(2001)040⟨0753:PBFTTB⟩2.0.CO;2.

Petersen, L., and F. Pellicciotti, 2011: Spatial and temporal variability of air temperature on a melting glacier: Atmospheric controls, extrapolation methods and their effect on melt modeling, Juncal Norte Glacier, Chile. *J. Geophys. Res.*, **116**, D23 109, doi:10.1029/2011JD015842.

Schirmer, M., and B. Jamieson, 2015: Verification of analysed and forecasted winter precipitation in complex terrain. *The Cryosphere*, **9**, 587–601, doi:10.5194/tc-9-587-2015.

Schwarb, M., 2000: The alpine precipitation climate: Evaluation of a high-resolution analysis scheme using comprehensive rain-gauge data. PhD dissertation, Swiss Federal Institute of Technoglogy (ETH) Zürich, 131 pp.

Stearns, C., and G. Weidner, 1993: Sensible and Latent Heat Flux Estimates in Antarctica. *Antarctic Meteorology and Climatology: Studies Based on Automatic Weather Stations. Antarctic Research Series*, **61**, 109–138, doi:DOI:10.1029/AR061p0109.

Vaughan, D., and Coauthors, 2013: *Observations: Cryosphere. In: Climate Change 2013: The Physical Science Basis. Contribution of Working Group I to the Fifth Assessment Report of the Intergovernmental Panel on Climate Change [Stocker, T.F., D. Qin, G.-K. Plattner, M. Tignor, S.K. Allen, J. Boschung, A. Nauels, Y. Xia, V. Bex and P.M. Midgley (eds.)].* Cambridge University Press, Cambridge, United Kingdom and New York, NY, USA, 317-382 pp., doi:10.1017/CBO9781107415324.013.

Vuille, M., B. Francou, P. Wagnon, I. Juen, G. Kaser, B. Mark, and R. Bradley, 2008: Climate change and tropical Andean glaciers: Past, present and future. *Earth-Sc. Rev.*, **89**, 79–96, doi:10.1016/j.earscirev.2008.04.002.

Wong, P., I. Losada, J.-P. Gattuso, J. Hinkel, A. Khattabi, K. McInnes, Y. Saito, and A. Sallenger, 2014: *Coastal systems and low-lying areas. In: Climate Change 2014: Impacts, Adaptation, and Vulnerability. Part A: Global and Sectoral Aspects. Contribution of Working Group II to the Fifth Assessment Report of the Intergovernmental Panel on Climate Change [Field, C.B., V.R. Barros, D.J. Dokken, K.J. Mach, M.D. Mastrandrea, T.E. Bilir, M. Chatterjee, K.L. Ebi, Y.O. Estrada, R.C. Genova, B. Girma, E.S. Kissel, A.N. Levy, S. MacCracken, P.R. Mastrandrea, and L.L. White (eds.)]*. Cambridge University Press, Cambridge, United Kingdom and New York, NY, USA, 361-409 pp.

Zemp, M., I. Gärtner-Roer, S. Nussbaumer, F. Hüsler, H. Machguth, N. Mölg, F. Paul, and M. Hoelzle, 2015: *WGMS 2015. Global Glacier Change Bulletin No. 1 (2012-2013)*. World Glacier Monitoring Service, Zurich, Switzerland, 230 pp., doi:10.5904/wgms-fog-2015-11.

Zemp, M., S. Nussbaumer, K. Naegeli, I. Gärtner-Roer, F. Paul, M. Hoelzle, and W. Haeberli (eds.), 2013: *WGMS 2013. Glacier Mass Balance Bulletin No. 12 (2010-2011)*. ICSU(WDS)/IUGG(IACS)/UNEP/UNESCO/WMO, World Glacier Monitoring Service, Zurich, Switzerland, 106 pp., doi:10.5904/wgms-fog-2013-11.

A INI-File Example

```
[GENERAL]
BUFF_CHUNK_SIZE = 370
BUFF_BEFORE = 1.5

[INPUT]
COORDSYS = UTM
COORDPARAM = 32T
TIME_ZONE = 0
METEO = SMET
METEOPATH = /home/peter/MA/modelruns/COSMO/VIR_sims/input/meteo
STATION1 = COSMO_P1.smet
STATION2 = COSMO_P2.smet
STATION3 = COSMO_P3.smet
STATION4 = COSMO_P4.smet
STATION5 = COSMO_P5.smet
STATION6 = COSMO_P6.smet

VIRTUAL_STATIONS = TRUE
VSTATION1 = 638300 5183526 32632
VSTATION2 = 638330 5183190 32632
VSTATION3 = 638380 5183010 32632
VSTATION4 = 638480 5182866 32632
VSTATION5 = 638580 5182672 32632
VSTATION6 = 638721 5182571 32632
VSTATION7 = 638821 5182471 32632
VSTATION8 = 638826 5182350 32632
VSTATION9 = 639010 5182420 32632
VSTATION10 = 638805 5182175 32632
VSTATION11 = 639107 5182274 32632
VSTATION12 = 638760 5182020 32632
VSTATION13 = 639140 5182185 32632
VSTATION14 = 638727 5181910 32632
VSTATION15 = 639188 5182115 32632
VSTATION16 = 638735 5181820 32632
VSTATION17 = 639280 5182045 32632
VSTATION18 = 639370 5181885 32632
```

```
VSTATION19 = 639551 5181839 32632

VIRTUAL_PARAMETERS = P TA RH VW DW PSUM ISWR ILWR
VSTATIONS_REFRESH_RATE = 3600
INTERPOL_USE_FULL_DEM = TRUE
ISWR_IS_NET = FALSE

SNOWPATH = /home/peter/MA/modelruns/COSMO/VIR_sims/input
SNOW = SMET
SNOWFILE1 = VIR01.sno
SNOWFILE2 = VIR02.sno
SNOWFILE3 = VIR03.sno
SNOWFILE4 = VIR04.sno
SNOWFILE5 = VIR05.sno
SNOWFILE6 = VIR06.sno
SNOWFILE7 = VIR07.sno
SNOWFILE8 = VIR08.sno
SNOWFILE9 = VIR09.sno
SNOWFILE10 = VIR10.sno
SNOWFILE11 = VIR11.sno
SNOWFILE12 = VIR12.sno
SNOWFILE13 = VIR13.sno
SNOWFILE14 = VIR14.sno
SNOWFILE15 = VIR15.sno
SNOWFILE16 = VIR16.sno
SNOWFILE17 = VIR17.sno
SNOWFILE18 = VIR18.sno
SNOWFILE19 = VIR19.sno

#reading ARC dem
DEM = ARC
DEMFILE = /home/peter/MA/modelruns/COSMO/VIR_sims/input/dem/GlacierArea.asc

[INTERPOLATIONS2D]
P::algorithms = STD_PRESS
TA::algorithms = IDW_LAPSE
TA::idw_lapse = -0.0055
RH::algorithms = LISTON_RH
VW::algorithms = LISTON_WIND
```

DW::algorithms = LISTON_WIND
PSUM::algorithms = PSUM_SNOW
PSUM::psum_snow = idw_lapse
PSUM::idw_lapse = 0.0005 frac
ISWR::algorithms = SWRAD
ILWR::algorithms = IDW_LAPSE
ILWR::avg_lapse = -0.029

[OUTPUT]
COORDSYS = UTM
COORDPARAM = 32T
TIME_ZONE = 0
METEO = SMET
METEOPATH = ./output
METEOPARAM = ASCII
WRITE_PROCESSED_METEO = TRUE
EXPERIMENT = shading
SNOW = SMET
BACKUP_DAYS_BETWEEN = 365.0
FIRST_BACKUP = 400.0
PROF_WRITE = FALSE
PROFILE_FORMAT = PRO
AGGREGATE_PRF = FALSE
PROF_START = 0.0
PROF_DAYS_BETWEEN = 0.041666
HARDNESS_IN_NEWTON = FALSE
CLASSIFY_PROFILE = FALSE
TS_WRITE = TRUE
TS_START = 0.0
TS_DAYS_BETWEEN = 0.041666
AVGSUM_TIME_SERIES = TRUE
CUMSUM_MASS = FALSE
PRECIP_RATES = TRUE
OUT_CANOPY = FALSE
OUT_HAZ = TRUE
OUT_SOILEB = FALSE
OUT_HEAT = TRUE
OUT_T = TRUE
OUT_LW = TRUE

```
OUT_SW = TRUE
OUT_MASS = TRUE
OUT_METEO = TRUE
OUT_STAB = TRUE

[SNOWPACK]
CALCULATION_STEP_LENGTH = 60
ROUGHNESS_LENGTH = 0.0044
HEIGHT_OF_METEO_VALUES = 2
HEIGHT_OF_WIND_VALUE = 10
ENFORCE_MEASURED_SNOW_HEIGHTS = FALSE
SW_MODE = INCOMING
ATMOSPHERIC_STABILITY = MO_MICHLMAYR
CANOPY = FALSE
MEAS_TSS = FALSE
CHANGE_BC = FALSE
THRESH_CHANGE_BC = -1.0
SNP_SOIL = TRUE
SOIL_FLUX = TRUE
GEO_HEAT = 0

[SNOWPACKADVANCED]
ASSUME_RESPONSIBILITY = AGREE
VARIANT = DEFAULT
ADJUST_HEIGHT_OF_METEO_VALUES = FALSE
ADJUST_HEIGHT_OF_WIND_VALUE = FALSE
SNOW_EROSION = FALSE
WIND_SCALING_FACTOR = 1.0
NUMBER_SLOPES = 1
PERP_TO_SLOPE = FALSE
ALLOW_ADAPTIVE_TIMESTEPPING = TRUE
FORCE_RH_WATER = TRUE
THRESH_RAIN = 1.2
THRESH_RAIN_RANGE = 0.0
THRESH_RH = 0.5
THRESH_DTEMP_AIR_SNOW = 3.0
HOAR_THRESH_RH = 0.97
HOAR_THRESH_VW = 3.5
HOAR_DENSITY_BURIED = 125.0
```

HOAR_MIN_SIZE_BURIED = 2.0
HOAR_DENSITY_SURF = 100.0
MIN_DEPTH_SUBSURF = 0.07
T_CRAZY_MIN = 120.0
T_CRAZY_MAX = 400.0
METAMORPHISM_MODEL = DEFAULT
NEW_SNOW_GRAIN_SIZE = 0.3
STRENGTH_MODEL = DEFAULT
VISCOSITY_MODEL = DEFAULT
SALTATION_MODEL = SORENSEN
WATERTRANSPORTMODEL_SNOW = BUCKET
WATERTRANSPORTMODEL_SOIL = BUCKET
SNOW_ALBEDO = PARAMETERIZED
ALBEDO_PARAMETERIZATION = LEHNING_0
SW_ABSORPTION_SCHEME = MULTI_BAND
HARDNESS_PARAMETERIZATION = MONTI
DETECT_GRASS = FALSE
PLASTIC = FALSE
JAM = FALSE
WATER_LAYER = FALSE
HEIGHT_NEW_ELEM = 0.02
MINIMUM_L_ELEMENT = 0.0025
COMBINE_ELEMENTS = TRUE
ADVECTIVE_HEAT = FALSE

B SNO-File Example

SMET 1.1 ASCII

[HEADER]
station_id = VIR1
station_name = Hochjochferner_VIR1
easting = 638300
northing = 5183526
epsg = 32632
altitude = 2724
nodata = -999
tz = 0
source = SNO-file with preconstructed glacier in ablation zone
ProfileDate = 2014-10-01T00:00:00
HS_Last = 0.0000
SlopeAngle = 0
SlopeAzi = 0
nSoilLayerData = 1
nSnowLayerData = 8
SoilAlbedo = 0.2
BareSoil_z0 = 0.020
CanopyHeight = 0.00
CanopyLeafAreaIndex = 0.00
CanopyDirectThroughfall = 1.00
WindScalingFactor = 1.00
ErosionLevel = 0
TimeCountDeltaHS = 0.000000
fields = timestamp Layer_Thick T Vol_Frac_I Vol_Frac_W Vol_Frac_V Vol_Frac_S Rho_S Conduc_S HeatCapac_S rg rb dd sp mk mass_hoar ne CDot metamo

[DATA]
1980-01-01T00:00 5 273.15 0.1 0 0 0.9 1000 1 2000000 0 0 0 0 0 0 1 0 0
2005-09-30T23:00 20 273.15 0.95 0.014 0.036 0 0 0 0 3 2.2 0 1 7 0 20 0 0
2008-09-30T23:00 10 273.15 0.95 0.014 0.036 0 0 0 0 3 2.2 0 1 7 0 20 0 0
2009-09-30T23:00 5 273.15 0.95 0.014 0.036 0 0 0 0 3 2.2 0 1 7 0 20 0 0
2010-09-14T23:00 1 273.15 0.95 0.014 0.036 0 0 0 0 1.5 1 0 1 7 0 10 0 0
2011-09-14T23:00 1 273.15 0.95 0.014 0.036 0 0 0 0 1.5 1 0 1 7 0 10 0 0

2012-09-14T23:00 1 273.15 0.95 0.014 0.036 0 0 0 0 1.5 1 0 1 7 0 20 0 0
2013-09-14T23:00 1 273.15 0.95 0.014 0.036 0 0 0 0 1.5 1 0 1 7 0 30 0 0
2014-09-14T23:00 1 273.15 0.95 0.014 0.036 0 0 0 0 1.5 1 0 1 7 0 50 0 0

Acknowledgments

First I want to thank my advisor Dr. Sascha Bellaire. Thank you for coming up with an idea when all I knew was that I wanted to do snowpack modelling, for all the meetings and your input, and also for your patience when I had to take long breaks from the project repeatedly. Another big thank you goes out to my secondary advisor Dr. Lindsey Nicholson, for all the spontaneous meetings, fresh viewpoints and for always providing me with supportive papers, figures and ideas.
Thank you also to Utrecht University's Institute for Marine and Atmospheric Research and to the Federal Office of Meteorology and Climatology MeteoSwiss for providing the data that made this thesis possible.
Of course, a very big thank you goes out to all my friends and colleagues from my time at the University and in Innsbruck; especially Stefan, Lukas, Andi and Sophie. I couldn't have asked for better company over the last years, it truly was an amazing time. Also thanks to Naschi for our early-morning missions during the final phase of this thesis, keeping the motivation high.
Thank you Babsi; over the time that this thesis developed, you certainly had the hardest job of all those mentioned here. Thanks for your endless encouragement, support, and for putting up with my various moods along the way.
Also thank you to the legendary old school crew Mathias, Christian and Stefan; it's been quite the journey, and apparently it's not over yet - life would not be the same without you.
And last, but not least, thank you to my family for all the amazing support you gave me; Helene and, of course, especially my parents; without you, none of this would have been possible.

Eidesstattliche Erklärung

Ich erkläre hiermit an Eides statt durch meine eigenhändige Unterschrift, dass ich die vorliegende Arbeit selbständig verfasst und keine anderen als die angegebenen Quellen und Hilfsmittel verwendet habe. Alle Stellen, die wörtlich oder inhaltlich den angegebenen Quellen entnommen wurden, sind als solche kenntlich gemacht.

Die vorliegende Arbeit wurde bisher in gleicher oder ähnlicher Form noch nicht als Magister-/Master-/Diplomarbeit/Dissertation eingereicht.

Datum	Unterschrift